NIMA-related kinase 9–mediated phosphorylation of the microtubule-associated LC3B protein at Thr-50 suppresses selective autophagy of p62/sequestosome 1

Received for publication, July 4, 2019, and in revised form, December 11, 2019 Published, Papers in Press, December 19, 2019, DOI 10.1074/jbc.RA119.010068

Birendra Kumar Shrestha[1], **Mads Skytte Rasmussen**[1], **Yakubu Princely Abudu, Jack-Ansgar Bruun, Kenneth Bowitz Larsen, Endalkachew A. Alemu, Eva Sjøttem, Trond Lamark, and Terje Johansen**[2]

From the Molecular Cancer Research Group, Department of Medical Biology, Faculty of Health Sciences, UiT–The Arctic University of Norway, 9037 Tromsø, Norway

Edited by George N. DeMartino

Human ATG8 family proteins (ATG8s) are active in all steps of the macroautophagy pathway, and their lipidation is essential for autophagosome formation. Lipidated ATG8s anchored to the outer surface of the phagophore serve as scaffolds for binding of other core autophagy proteins and various effector proteins involved in trafficking or fusion events, whereas those at the inner surface are needed for assembly of selective autophagy substrates. Their scaffolding role depends on specific interactions between the LC3-interacting region (LIR) docking site (LDS) in ATG8s and LIR motifs in various interaction partners. LC3B is phosphorylated at Thr-50 within the LDS by serine/threonine kinase (STK) 3 and STK4. Here, we identified LIR motifs in STK3 and atypical protein kinase Cζ (PKCζ) and never in mitosis A (NIMA)-related kinase 9 (NEK9). All three kinases phosphorylated LC3B Thr-50 *in vitro*. A phospho-mimicking substitution of Thr-50 impaired binding of several LIR-containing proteins, such as ATG4B, FYVE, and coiled-coil domain-containing 1 (FYCO1), and autophagy cargo receptors p62/sequestosome 1 (SQSTM1) and neighbor of BRCA1 gene (NBR1). NEK9 knockdown or knockout enhanced degradation of the autophagy receptor and substrate p62. Of note, the suppression of p62 degradation was mediated by NEK9-mediated phosphorylation of LC3B Thr-50. Consistently, reconstitution of LC3B-KO cells with the phospho-mimicking T50E variant inhibited autophagic p62 degradation. PKCζ knockdown did not affect autophagic p62 degradation, whereas STK3/4 knockouts inhibited autophagic p62 degradation independently of LC3B Thr-50 phosphorylation. Our findings suggest that NEK9 suppresses LC3B-mediated autophagy of p62 by phosphorylating Thr-50 within the LDS of LC3B.

Macroautophagy (hereafter referred to as autophagy) is an evolutionarily-conserved pathway for degradation of cytosolic components (1). Autophagy begins with the formation of a crescent-shaped membrane structure termed the phagophore. The phagophore grows to envelop cytosolic content resulting in the formation of a closed, double-membrane structure surrounding the content, the autophagosome. The autophagosome might fuse with late endosomes before ultimately fusing with lysosomes forming an autolysosome, in which the content is degraded (2). Autophagy can either be nonspecific, *i.e.* degradation of long-lived cytosolic proteins, termed bulk autophagy or selective, *i.e.* targeted degradation of specific proteins and organelles (3). Selective autophagy is involved in the degradation of a diverse range of cytosolic components, including mitochondria (mitophagy), peroxisomes (pexophagy), protein aggregates (aggrephagy), bacteria (xenophagy), and the endoplasmic reticulum (reticulophagy) (4). Selective autophagy relies on a number of cargo receptors of which the most well-studied is p62/SQSTM1 (sequestosome-1) (5, 6). These cargo receptors interact with ATG8 proteins through the LC3-interacting region (LIR)[3] motif, which tethers the cargo receptors, along with their cargo, to the phagophore (7).

Core to the autophagic pathway is the ATG8 family of proteins (ATG8s) that, except for an N-terminal arm, structurally resemble the ubiquitin family of proteins (8). The mammalian ATG8 family consists of seven members subdivided into two families: MAP1LC3/LC3 (microtubule-associated protein 1 light chain 3) -A, -B, -B2, and -C and GABA receptor-associated proteins (GABARAP), GABARAPL1 (GABA A receptor-associated protein-like 1) and GABARAPL2. Newly-synthesized ATG8s are processed by the cysteine protease family ATG4 exposing a C-terminal glycine (9). In a manner analogous to the ubiquitin system, ATG8s are first activated by ATG7 (E1-like), transferred to ATG3 (E2-like), before finally becoming covalently attached to phosphatidylethanolamine (PE) by the action of the ATG12–ATG5–ATG16 complex (E3-like), enabling

This work was supported by FRIBIOMED Program Grant 214448 and TOPPFORSK Program Grant 249884 of the Research Council of Norway and Norwegian Cancer Society Grant 71043-PR-2006-0320 (to T. J.). The authors declare that they have no conflicts of interest with the contents of this article.

This article contains Figs. S1–S4 and Table S1.

The MS proteomics data have been deposited to the ProteomeXchange Consortium via the PRIDE partner repository with the dataset identifier accession no. PXD016681.

[1] Both authors contributed equally to this work.

[2] To whom correspondence should be addressed. Tel.: 47 77644720; E-mail: terje.johansen@uit.no.

[3] The abbreviations used are: LIR, LC3-interacting region; CLIR, C-type LIR; LDS, LC3-docking site; PKC, protein kinase C; NIMA, Never in Mitosis A; PE, phosphatidylethanolamine; GABA, γ-aminobutyric acid; GABARAP, GABA receptor-associated protein; DMEM, Dulbecco's modified Eagle's medium; ETD, electron transfer dissociation; LDH, lactate dehydrogenase; AR, autoradiography; ANOVA, analysis of variance; EGFP, enhanced GFP; CBB, Coomassie Brilliant Blue; PDB, Protein Data Bank; HBSS, Hanks' balanced salt solution; PTM, post-translational modification; STK, serine/threonine kinase; mTOR, mechanistic target of rapamycin; GST, glutathione *S*-transferase; CID, collision-induced dissociation.

membrane attachment (10). ATG8s are released from the phagophore, and from the outer membrane of the autophagosome, by ATG4-mediated cleavage of the ATG8–PE bond, thereby restoring free ATG8 (11). The ATG8s have been shown to be involved in the nucleation, expansion (12), and closure of the phagophore (13).

The ATG8s coat the inner and outer membrane of the phagophore (14) and function as anchoring points for the autophagic machinery as well as recruitment of cargo receptors to the phagophore (7). A growing number of protein interactions involving ATG8s have been shown to be mediated through an LIR motif on the binding partner of ATG8, which interacts with the LIR-docking site (LDS) on the ATG8s (15). The LDS consists of two hydrophobic pockets (HP1 and -2) capable of encompassing the core residues of the consensus LIR sequence separated by two variable amino acids ((W/F/Y)*XX*(L/I/V)) (16). Another type of LIR motif termed C-type LIR (CLIR) has also been shown to bind LC3C through interaction with HP2 (17). LIR motifs are very often flanked N-terminally by acidic residues that interact with basic residues in the N-terminal α-helix of ATG8s (15). The variation within the LIR motif sequence determines preferential binding to individual ATG8 family members and determines binding affinity and thereby competitive interaction with other LIR motif-containing autophagic proteins. Such binding specificity might regulate the autophagy pathway (15). The autophagy pathway is tightly regulated by several autophagy-related proteins. Among such regulatory proteins are kinases such as ULK1 (unc-51-like autophagy activating kinase 1) and ULK2 and mechanistic target of rapamycin (mTOR) (18). Several other serine-threonine kinases were identified as interactors of the ATG8 family proteins in a human autophagy interactomics study (19). NEK9 belongs to the NIMA (Never in Mitosis A)-related kinase family. Members of the NIMA family are associated with cell cycle–related functions during mitosis. Specifically, NEK9 plays an essential role in the assembly of spindle fibers early in mitosis (20). STK3 (serine/threonine-protein kinase 3) and STK4 play an essential role in the Hippo signaling pathway. STK3 and STK4 act as negative regulators of transcription co-activators YAP1 (Yes-associated protein 1) and WWTR1 (WW domain-containing transcription regulator 1 (WWTR1). YAP1 and WWTR1 are associated with genes that regulate cell proliferation, survival, and differentiation (21). Besides its role as a tumor suppressor, loss of STK4 leads to high susceptibility toward infection likely due to loss of immune cells (B and T lymphocytes) (22, 23). STK4 was first reported as a negative regulator of autophagy. STK3 was shown to negatively regulate autophagy via phosphorylation of Beclin 1 at Thr-108, thereby promoting interaction between Beclin 1 and Bcl-2 (24). The role of atypical protein kinase C in autophagy is less understood. Recently, protein kinase Cι (PKCι) was shown to negatively regulate autophagy via direct phosphorylation-mediated activation of PI3 kinase–AKT–mTOR-signaling pathway (25).

Several post-translational modifications (PTMs) have been reported in LC3B both surrounding the core LDS as well as in the N-terminal arm (26). Phosphorylation of threonine 6 (Thr-6) and Thr-29 in the N-terminal arm of LC3B by PKC has been reported but was found to have no effect on overall autophagy or LC3B processing (27). Several other studies have reported PTMs near the LDS, including phosphorylation of Thr-50 (28), as well as acetylation of lysine 49 (Lys-49) and Lys-51 (29). Phosphorylation of Thr-50 by STK3 and -4 is reported to be required for proper autophagosome–lysosome fusion (28). Furthermore, STK3$^{+/-}$/STK4$^{-/-}$ knockout cells display deficient xenophagy, as these cells are unable to efficiently clear intracellular bacteria (28). Acetylation of Lys-49 and Lys-51 is reported to cause nuclear retention of LC3B in full medium. Upon starvation, LC3B is deacetylated by SIRT1 and transported out of the nucleus by DOR/TP53INP2. This shuttling was found to be crucial for the ability of LC3B to form puncta, most likely representing autophagosomes, in the cytosol (29).

Given the proximity to the LDS, we hypothesized that phosphorylation of Thr-50 could regulate the interaction between LC3B and LIR-containing proteins. To this end, we used CRISPR/Cas9 technology to establish a Flp-In T-Rex HEK293 LC3B knockout (KO) cell line. By stably reconstituting the LC3B KO cell line with LC3B WT, -T50A, -T50E, and LC3B F52A/L53A (LDS mutants), we found that selective autophagic flux was strongly inhibited by both T50E and F52A/L53A mutations. Furthermore, the phospho-mimicking LC3B T50E mutant displayed significantly reduced interaction with several essential autophagy-related proteins such as p62/SQSTM1(sequestosome-1), ATG7, ATG4B, FYCO1, and Syntaxin-17. By *in vitro* phosphorylation assays, we identified NEK9 as a potential kinase that mediates phosphorylation of LC3B Thr-50. Interestingly, the KD of NEK9 led to enhanced autophagic flux in WT cells but had no effect on LC3B KO cells reconstituted with mutant LC3B T50A/T50E. This result suggests that NEK9 regulates autophagy involving LC3B by phosphorylation of Thr-50 within the LDS.

Results

STK3 interacts with LC3C and GABARAP via a CLIR

The pioneering proteomic analysis of the autophagy interaction network in human cells by Behrends *et al.* (19) revealed several serine/threonine kinases as part of the ATG8s interactome, including STK3, STK4, NEK9, and PKCζ. The major autophagy regulating protein kinases ULK1 and -2 (30) and the yeast orthologue Atg1 (31) have been shown to bind to ATG8s and to do so via LIR motifs. To study whether NEK9, PKCζ, STK3, and -4 engage in LIR-dependent interactions with ATG8s, we first validated that they are bound to LC3B *in vivo*. NEK9, PKCζ, and STK3/4 were transiently co-expressed with GABARAP or LC3B in HEK293 cells. The kinases were immunoprecipitated and co-precipitated ATG8s detected by Western blotting (Fig. 1*A*). For this purpose, we used both a functional kinase (WT) and a kinase-deficient mutant (KD) (Fig. S1*A*). Previously, mutations in the Mg^{2+}-binding motif (DFG) or the ATP-binding motif (VAIK) of PKCs, which both abolish ATP binding, have been shown to cause apoptotic effects *in vivo* (32). We therefore chose to mutate the aspartic acid of the His–Arg–Asp (HRD) motif necessary for proton transfer from the serine/threonine residue. Both GFP–LC3B and GFP–GABARAP co-immunoprecipitated with all the tested kinases independent of their kinase activity. Albeit the kinase-dead vari-

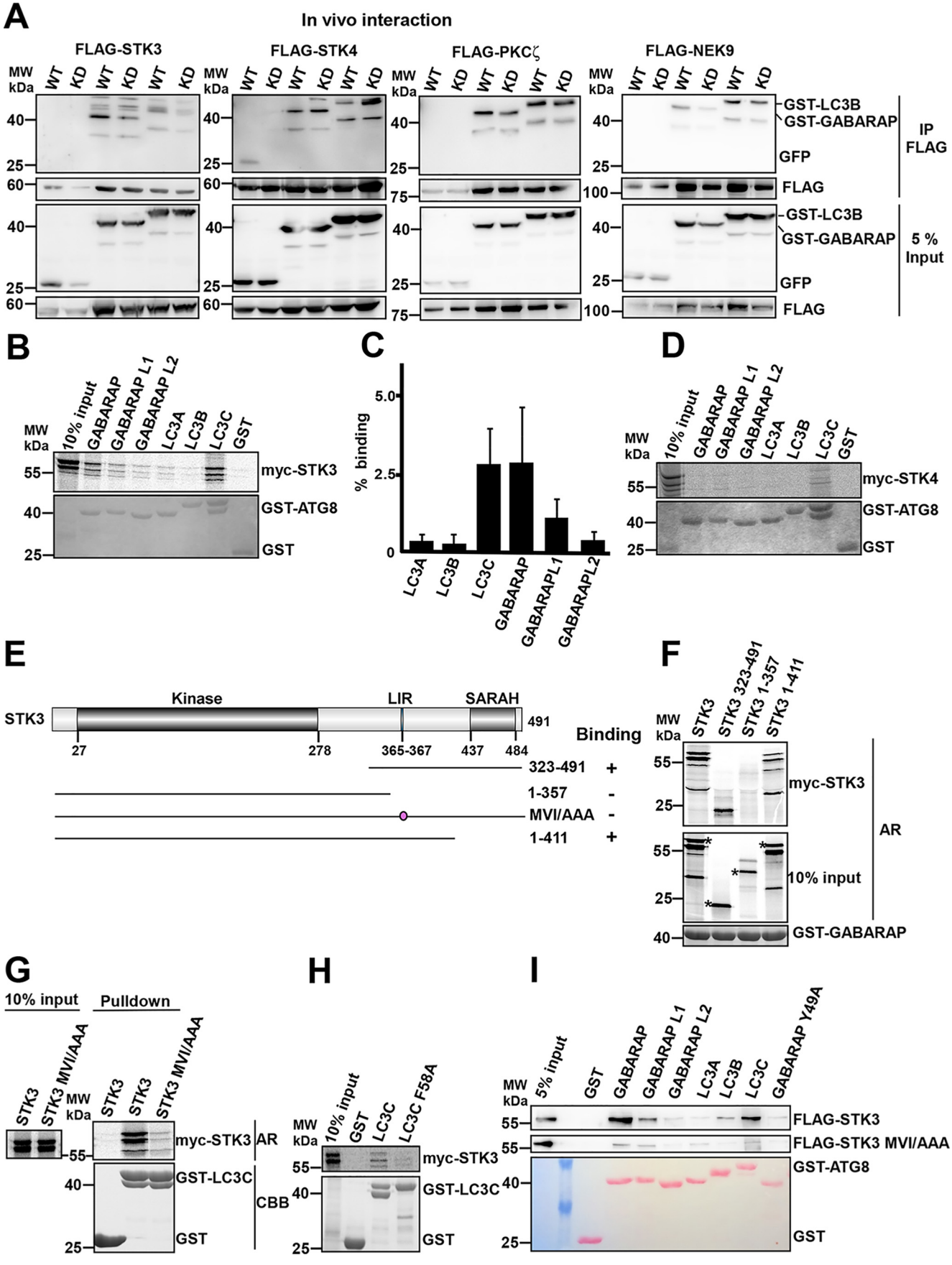
A
In vivo interaction
FLAG-STK3
FLAG-STK4
FLAG-PKCζ
FLAG-NEK9
MW kDa
WT KD WT KD WT KD
GST-LC3B
GST-GABARAP
GFP
FLAG
IP FLAG
5 % Input
B
10% input
GABARAP
GABARAP L1
GABARAP L2
LC3A
LC3B
LC3C
GST
myc-STK3
GST-ATG8
GST
C
% binding
LC3A
LC3B
LC3C
GABARAP
GABARAPL1
GABARAPL2
D
myc-STK4
E
STK3
Kinase
LIR
SARAH
491
27
278
365-367
437
484
Binding
323-491 +
1-357 -
MVI/AAA -
1-411 +
F
STK3
STK3 323-491
STK3 1-357
STK3 1-411
myc-STK3
AR
10% input
GST-GABARAP
G
10% input
Pulldown
STK3 MVI/AAA
myc-STK3
AR
GST-LC3C
CBB
GST
H
10% input
GST
LC3C
LC3C F58A
I
5% input
GABARAP Y49A
FLAG-STK3
FLAG-STK3 MVI/AAA
GST-ATG8

ants of STK3 and NEK9 bound slightly less to both GABARAP and LC3B in the experiments shown (Fig. 1*A*), this was not consistently observed. Of note, co-expression of the GFP tag alone with the kinases caused apoptosis leading to a low yield of STK3 and -4, PKCζ, and NEK9, as reported previously (33).

To further characterize the interaction between the kinases and ATG8 family proteins, we first addressed the interactions between the hippo kinases and ATG8 family proteins. To this end, GST–pulldown assays using translated *in vitro* STK3 showed that STK3 interacted directly with several of the ATG8s, but most strongly with LC3C and GABARAP and more weakly with GABARAPL1 (Fig. 1, *B* and *C*). However, STK4 interacted very weakly with the ATG8s (Fig. 1*D*). STK3 contains an N-terminal kinase domain followed by an unstructured region important for inhibition of the kinase activity by covering the active site. In the far C-terminal region resides the SARAH domain, which is important for dimerization (Fig. 1*E*) (34). A caspase-3 cleavage site (Asp-322) is located at position Asp-322 which, if cleaved, produces a C-terminally truncated, activated version of STK3 (35). To map the binding site for ATG8 on STK3, we established expression constructs corresponding to the fragment produced by caspase cleavage *in vivo* as well as various C-terminally–deleted constructs (Fig. 1*E*). GST pulldown assays using the various deletion constructs of STK3 identified the interaction to be mediated by the fragment encompassing the C-terminal region from amino acid position 323, and not the N-terminal part (from position 1 to 357) (Fig. 1*F*). GABARAP was used as an interaction partner in these LIR-mapping experiments because it bound strongly to STK3. However, because STK3 also bound strongly to LC3C, we searched the C-terminal part of STK3 for CLIR with the consensus ΦΦΦ, where Φ is an aliphatic amino acid. A candidate CLIR, "MVI" was located at positions 365–367, reminiscent of the CLIR previously described for the interaction between CALCOCO2/NDP52 and LC3C (36). Strikingly, mutation of this CLIR motif to AAA abolished binding between STK3 and LC3C (Fig. 1*G*). Consistently, mutation of the LDS in LC3C F58A resulted in a strongly-decreased binding to STK3 (Fig. 1*H*). GST-pulldown assays using extracts from HeLa cells expressing the FLAG–STK3 or the FLAG–STK3 MVI/AAA CLIR mutant verified the strong binding of FLAG–STK3 to GABARAP and LC3C, whereas the CLIR mutant FLAG–STK3 MVI/AAA did not show significant binding. Furthermore, the GABARAP Y49A LDS mutant displayed strongly-reduced binding to FLAG–STK3 (Fig. 1*I*). Taken together, the results show that the CLIR motif in STK3 mediated LDS-dependent binding to both LC3C and GABARAP.

PKCζ binds to GABARAP and GABARAPL1 via an LIR motif overlapping with the AGC kinase docking motif

The atypical PKCs contain a C-terminal kinase domain whose activity is regulated by the N-terminal region composed of an N-terminal Phox and Bem1p (PB1) domain, followed by a C1-like zinc finger domain, which is preceded by a pseudosubstrate peptide (Fig. 2*A*). We conducted a peptide array screen to probe the entire PKCζ for any LIR-like motifs (37). Three candidate motifs were identified (Fig. 2*B*). Because there are no 3D structures available for PKCζ, we used the structure of PKCι (Protein Data Bank code 3A8W) to assess whether the motifs that were positive hits from the peptide array were likely to be exposed on the surface of PKCζ. The motif "DIDWVQ" is located in a solvent-exposed part of the kinase domain of PKCζ/ι, in an α-helical structure with the aromatic tryptophan pointing inward toward the ATP-binding pocket. "WDLL" (WDMM in PKCι) is located just C-terminal to the kinase domain and is solvent-exposed in the structure; however, tryptophan is facing inward between the two α-helices. The motif showing the strongest binding in the peptide array "FEYI" overlaps with the AGC kinase–docking motif (FEGFEYI), important for the binding and activation of PKCζ/ι by PDK1 (38), and it is located in a solvent-exposed region in the far C-terminal part of PKCζ/ι. However, again the aromatic phenylalanine is pointing inward in the structure. Mutation of the aromatic Phe residue in the FEYI core sequence in a peptide covering the C-terminal part of PKCζ prevented the interaction with GABARAP, and mutation of the hydrophobic Ile residue strongly reduced binding (Fig. 2*C*). This supports that FEYI might be a functional LIR motif. This was confirmed by GST-pulldown assays with full-length PKCζ with both the aromatic and hydrophobic residues in the core LIR mutated to alanines, which strongly inhibited binding to the ATG8s both *in vitro* (Fig. 2, *D* and *E*) and in cell extracts (Fig. 2*F*). PKCζ bound most strongly to GABARAP and GABARAPL1 *in vitro* (Fig. 2*E*), and in lysates from HEK293 cells transfected with EGFP–PKCζ (Fig. 2*F*). PKCζ did not interact with LC3C. The interaction with LC3B *in vitro* and *in vivo* was very weak (Fig. 2, *D–F*), although LC3B is efficiently immunoprecipitated with PKCζ from cell extracts (Fig. 1*A*). This suggests that either PTMs of LC3B or PKCζ are required for efficient binding or the association is not direct, *i.e.* they are part of a larger complex. Confirming that PKCζ bound via an LIR–LDS interaction, a sim-

Figure 1. STK3 interacts with LC3C and GABARAP via a C-type atypical LIR motif. *A*, HEK293 cells were transiently co-transfected with the indicated FLAG-tagged kinases, wildtype (*WT*), or kinase-dead (*KD*), and either GFP–LC3B or GFP-GABARAP. Cell lysates were immunoprecipitated (*IP*) with FLAG antibodies and analyzed by Western blotting. *B*, Myc-tagged STK3 kinase constructs were translated *in vitro* in the presence of [^{35}S]methionine and analyzed in GST affinity isolation experiments for binding to the indicated ATG8s fused to GST. Bound proteins were detected by autoradiography and immobilized GST or GST-tagged proteins visualized by Coomassie Brilliant Blue staining. *C*, quantification of STK3 binding shown in *B* and based on three independent experiments. Values are mean ± S.E. *D*, Myc-tagged STK4 kinase construct was translated *in vitro* in the presence of [^{35}S]methionine and analyzed in GST affinity isolation experiments for binding to the indicated ATG8s fused to GST. *E*, schematic drawing of the domain organization of STK3 with the kinase domain, the LIR motif, and the SARAH domain indicated. The extent of deletion mutants and the location of the MVI/AAA LIR mutation are shown *below* the domain cartoon. *F*, GST pulldown analyses of binding of the Myc-tagged STK3 deletion constructs shown in *E* to GST–GABARAP. The deletion constructs were translated *in vitro* in the presence of [^{35}S]methionine. *G*, and *H*, GST pulldown analyses of binding of Myc-tagged STK3 WT and LIR mutant translated *in vitro* in the presence of [^{35}S]methionine to GST-LC3C (*G*) or Myc-tagged STK3 WT translated *in vitro* in the presence of [^{35}S]methionine to GST-LC3C or GST-LC3C F58A (*H*). The F58A mutant inhibits binding to the LDS of LC3C. *I*, HEK293 cells were transiently transfected with FLAG-tagged constructs of STK3 WT and LIR mutant (MVI/AAA), and whole-cell lysates were incubated with recombinant GST or GST–ATG8s family proteins. The bound FLAG-tagged STK3 protein was detected by Western blotting using anti-FLAG antibodies and immobilized GST or GST-tagged proteins visualized by Ponceau S staining. *AR*, autoradiography; *CBB*, Coomassie Brilliant Blue.

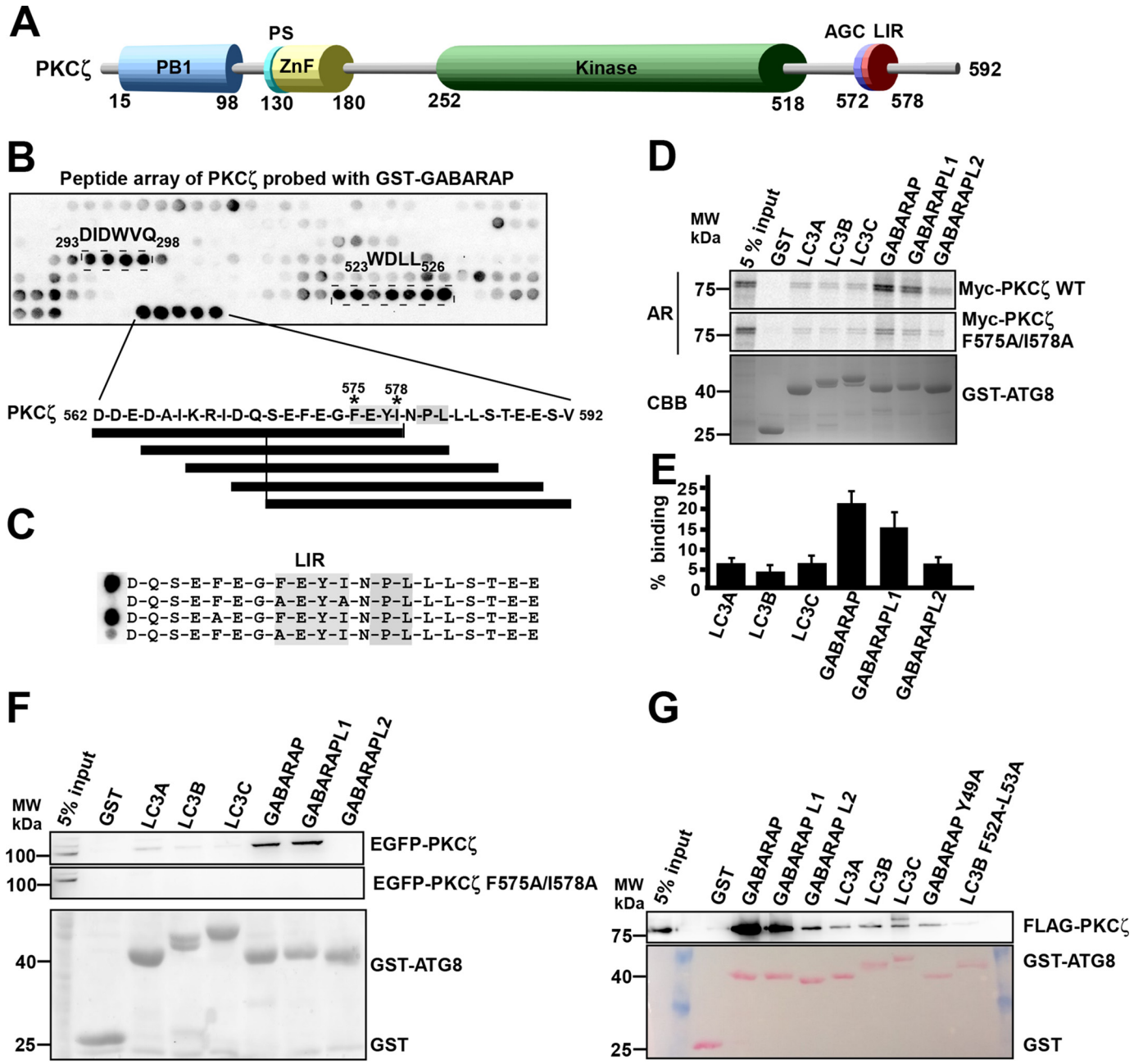

Figure 2. PKCζ binds to GABARAP and GABARAPL1 via a LIR motif overlapping with the AGC kinase docking motif. *A*, schematic diagram of the domain organization of PKCζ with the N-terminal PB1 domain involved in heterodimerization, the pseudosubstrate sequence (*PS*), the zinc finger domain (*ZnF*), the kinase domain, and the overlapping AGC kinase docking and LIR motifs. *B*, identification of GABARAP-binding putative LIR motifs in PKCζ. An array of 20-mer peptides covering full-length PKCζ (each peptide shifted three amino acids relative to the previous) was mixed with GST–GABARAP (1 μg/ml) and binding detected using ant-GST antibodies. The extensions of the most strongly interacting peptides are indicated, of which the overlapping peptides harboring the FEYI core LIR motif clearly bound most strongly. *C*, peptide array performed as in *B* but with the 20-mer harboring the FEYI motif with or without the core phenylalanine (*F*) and/or isoleucine (*I*) residues mutated to alanine and a more N-terminal F mutated to Ala. *D*, Myc-tagged PKCζ WT and LIR mutant (F575A/I578A) constructs were translated *in vitro* in the presence of [^{35}S]methionine and tested in GST affinity isolation experiments for binding to human ATG8 family proteins. Bound proteins were detected by autoradiography (*AR*) and immobilized GST or GST-tagged proteins by CBB. *E*, quantification of the binding of WT Myc-PKCζ to GST–ATG8s. Values are mean ± S.E. *F*, HEK293 cells were transiently transfected with EGFP-tagged WT and LIR mutant (F575A/I578A) PKCζ expression constructs and whole-cell lysates were incubated with recombinant GST or GST–ATG8 family proteins. The bound EGFP-tagged PKCζ proteins were detected by Western blotting using anti-EGFP antibodies and immobilized GST or GST-tagged proteins visualized by Ponceau S staining. *G*, similar experiment as in *F* but with FLAG-tagged PKCζ and GST–ATG8 proteins, including the LDS mutants GABARAP Y49A and LC3B F52A/L53A. The bound FLAG-tagged PKCζ protein was detected by Western blotting using anti-FLAG antibodies and immobilized GST or GST-tagged proteins visualized by Ponceau S staining.

ilar pulldown experiment as in Fig. 2*F* was performed using extracts from HEK293 cells transfected with FLAG-tagged PKCζ and GST–ATG8 proteins, including the LDS mutants GABARAP Y49A and LC3B F52A/L53A. The LDS mutants showed strongly reduced binding to FLAG-PKCζ (Fig. 2*G*).

NEK9 interacts with ATG8s via a C-terminal LIR motif

NEK9 comprises an N-terminal kinase domain, an RCC1 (regulator of chromatin condensation)-like β-propeller domain with six RCC repeats followed by a C-terminal domain with an unstructured region that binds to NEK6 and a coiled-coil region (Fig. 3*A*).

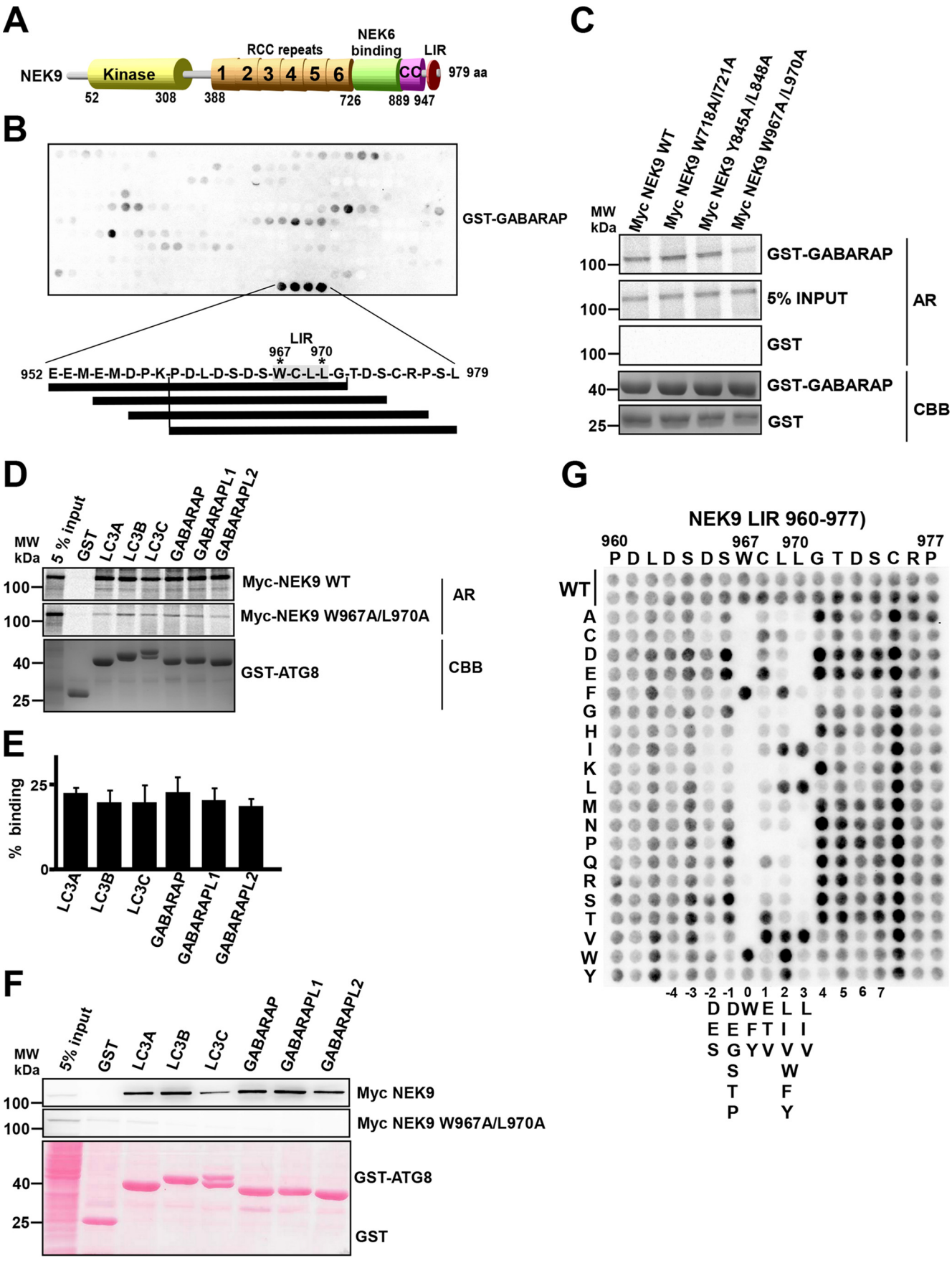
A
NEK9
Kinase
RCC repeats
1 2 3 4 5 6
NEK6 binding
CC
LIR
979 aa
52
308
388
726
889 947
B
GST-GABARAP
LIR
967 970
952 E-E-M-E-M-D-P-K-P-D-L-D-S-D-S-W-C-L-L-G-T-D-S-C-R-P-S-L 979
C
MW kDa
Myc NEK9 WT
Myc NEK9 W718AI721A
Myc NEK9 Y845A /L848A
Myc NEK9 W967A /L970A
100
GST-GABARAP
100
5% INPUT
100
GST
AR
40
GST-GABARAP
25
GST
CBB
D
MW kDa
5 % input
GST
LC3A
LC3B
LC3C
GABARAP
GABARAPL1
GABARAPL2
100
Myc-NEK9 WT
100
Myc-NEK9 W967A/L970A
AR
40
GST-ATG8
25
CBB
E
% binding
25
0
LC3A
LC3B
LC3C
GABARAP
GABARAPL1
GABARAPL2
F
MW kDa
5% input
GST
LC3A
LC3B
LC3C
GABARAP
GABARAPL1
GABARAPL2
100
Myc NEK9
100
Myc NEK9 W967A/L970A
40
GST-ATG8
25
GST
G
NEK9 LIR 960-977)
960
967
970
977
P D L D S D S W C L L G T D S C R P
WT
A C D E F G H I K L M N P Q R S T V W Y
-4 -3 -2 -1 0 1 2 3 4 5 6 7
D D W E L L
E E F T I I
S G Y V V V
S W
T F
P Y

To identify putative LIR motifs within NEK9, we employed the iLIR prediction server (39) and peptide array screening methods (37). The iLIR server predicted three putative C-terminal LIR motifs: ^{718}WHTI^{721}, ^{845}YEEL^{848}, and ^{967}WCLL^{970}, whereas the peptide array revealed only the most C-terminal LIR motif as a candidate ATG8-binding domain (Fig. 3*B*). To determine whether any of the predicted LIR motifs mediated the ATG8s interaction, the aromatic and hydrophobic residues of the putative core LIRs were mutated to alanine in the three predicted LIRs. NEK9 WT and the three mutants were assayed for GABARAP binding in a GST-pulldown assay. The NEK9 W967A/L970A mutant displayed strongly-reduced binding with GST GABARAP, whereas the other mutations did not affect binding at all (Fig. 3*C*). GST-pulldown assay with in vitro–translated NEK9 showed that WT NEK9 interacted very well with all ATG8s, whereas the W967A/L970A LIR mutant lost almost all binding to the ATG8s (Fig. 3*D*). Strikingly, NEK9 bound with equal affinity to all six ATG8 family proteins (Fig. 3*E*). A similar binding pattern was seen in GST-pulldown assays, with whole-cell lysates from HeLa cells transiently transfected with Myc-tagged NEK9 WT and NEK9 LIR mutant constructs incubated with recombinant GST or GST–ATG8s beads. All ATG8 proteins bound well, although the LIR mutation abolished binding (Fig. 3*F*). In conclusion, NEK9 contains a C-terminal LIR motif with the core LIR sequence ^{967}WCLL^{970}.

To further analyze the sequence requirements for binding to GABARAP of the C-terminal LIR of NEK9, a two-dimensional peptide array mutation analysis was performed. Each position of an 18-mer NEK9 peptide encompassing amino acids 960–977 was substituted with all 19 alternative amino acids, and the array was probed with GST–GABARAP (Fig. 3*G*). The results confirm the absolute requirements of an aromatic residue at position 0 and either Leu, Ile, or Val at the hydrophobic position +3. Tyr is not as efficient in replacing Trp as Phe at position 0. Apart from the invariant aromatic and hydrophobic positions of the core LIR, the intermediate +1 and +2 positions also show clear preference for allowed substitutions. The rather unusual Cys at position +1 is most effectively replaced by Glu, Val, or Thr, whereas the Leu at +2 is only productively substituted by the hydrophobic Ile or Val and the aromatic residues (Trp, Phe, and Tyr). As almost always seen (15, 30), basic residues (Arg and Lys) and proline and glycine are selected against in the core LIR. Interestingly, there are serines at the −1 and −3 positions suggesting that LIR binding can be positively regulated by phosphorylation. There are also acidic residues at positions −2 and −4 that are often involved in electrostatic interactions with N-terminal residues of the ATG8s (15). Position −1 shows a preference for either acidic Ser, Thr, Pro, or Gly residues. These residues are most often found in this position (15, 40). Position −2 also shows a strong preference for acidic (Asp and Glu) or Ser residues. At position +4 C-terminal to the core LIR, Cys, aromatic, and hydrophobic residues (Leu, Ile, and Val) are detrimental to the binding. There is a tendency for counterselection of these residues in the following +5 to +7 positions as well. A recent study of determinants regulating the selective binding of autophagy adapters and receptors to ATG8 proteins allows us to speculate that the fact that NEK9 binds so well to LC3B may perhaps be explained by favorable residues for LC3B binding located at +2 and −1 and −2 of the NEK9 LIR (40).

LC3B is phosphorylated in vitro by STK3, STK4, NEK9, and PKCζ

Recently, the hippo kinases STK3 and STK4 were shown to phosphorylate LC3B on Thr-50 leading to enhanced autophagosome–lysosome fusion (28). Thus, we asked whether NEK9 and PKCζ, which we show bind to ATG8s via LIR–LDS interactions, are also similarly able to phosphorylate LC3B at Thr-50. STK3 and -4 were included as positive controls. We constructed a GST–LC3B T50A nonphosphorylatable mutant and conducted *in vitro* kinase assays. PKCζ as well as NEK9 were able to phosphorylate LC3B and interestingly exhibited less phosphorylation when probed against LC3B T50A (Fig. 4, *A* and *B*). As reported previously (28), both hippo kinases were able to phosphorylate LC3B and displayed reduced phosphorylation of LC3B T50A (Fig. 4, *A* and *B*). As a control, PTEN-induced kinase 1 (PINK1) was not able to phosphorylate LC3B, although it phosphorylated its known substrate ubiquitin (Fig. 4*C*). To validate that STK3, STK4, NEK9, and PKCζ phosphorylates LC3B at Thr-50 and that the reduced phosphorylation of LC3B T50A is not a result of interference with the structural integrity of LC3B, we chose to employ MS. We performed *in vitro* kinase assays on GST-tagged LC3B, and the phosphorylated GST–LC3B was excised from the gel and subjected to in-gel chymotrypsin digestion before analysis by HPLC-tandem MS (HPLC-MS/MS) to map the phosphorylations sites (Fig. 4*D* and Table S1). Although several other sites were identified as phosphorylated, threonine 50 was by far the major phosphorylated site by NEK9 and STK4. It was also, along with Thr-6, the most efficiently phosphorylated site by STK3. Thr-50 was also phosphorylated by PKCζ, but not so efficiently (Fig. 4*D*). All sites shown in Fig. 4*D* were identified as high-confidence sites. As an example, the data for identification of Thr-50 phosphorylation by NEK9 is shown in Fig. S2.

Figure 3. NEK9 interacts with ATG8s via a C-terminal LIR motif. *A*, schematic diagram of NEK9 domain structure comprising the N-terminal kinase domain, the regulator of chromosome condensation 1(RCC1) repeats, a NEK6-binding region, a coiled-coil domain (*CC*), and the C-terminal LIR motif. *B*, identification of GABARAP-binding LIR motifs in the C terminus of NEK9. An array of 20-mer peptides, moved increments of three amino acids (*aa*), covering the entire 979-amino acid–long sequence of NEK9 was probed with GST–GABARAP (1 μg/ml), and binding was detected using anti-GST antibodies. The sequences of the overlapping peptides giving a positive signal are shown *below* the array with the core LIR motif *WCLL* indicated. *C*, Myc-tagged NEK9 LIR mutant constructs were translated *in vitro*, labeled with [^{35}S]methionine, and analyzed for binding to GST–GABARAP. *D*, GST pulldown assays with *in vitro*-translated and [^{35}S]methionine-labeled Myc-tagged NEK9 WT and LIR mutant W967A/L970A and GST–ATG8 proteins. Bound proteins were detected by AR, and immobilized GST or GST-tagged proteins by CBB staining. *E*, quantification of the binding of WT Myc-NEK9 to ATG8 family proteins. Values are mean ± S.E. *F*, GST pulldown assay, where Myc-tagged NEK9 WT and NEK9 LIR mutant constructs were transiently transfected into HeLa cells. The whole-cell lysates were incubated with recombinant GST or GST–ATG8s beads and bound NEK9 was detected by immunoblotting using anti-NEK9 antibody. The GST and GST–ATG8 proteins were visualized by Ponceau S staining. *G*, two-dimensional peptide array to investigate effects of single amino acid substitution at all positions of an 18-mer peptide from NEK9(960–977) harboring the LIR motif. The array was probed with GST–GABARAP (1 μg/ml), and binding was detected using anti-GST antibodies.

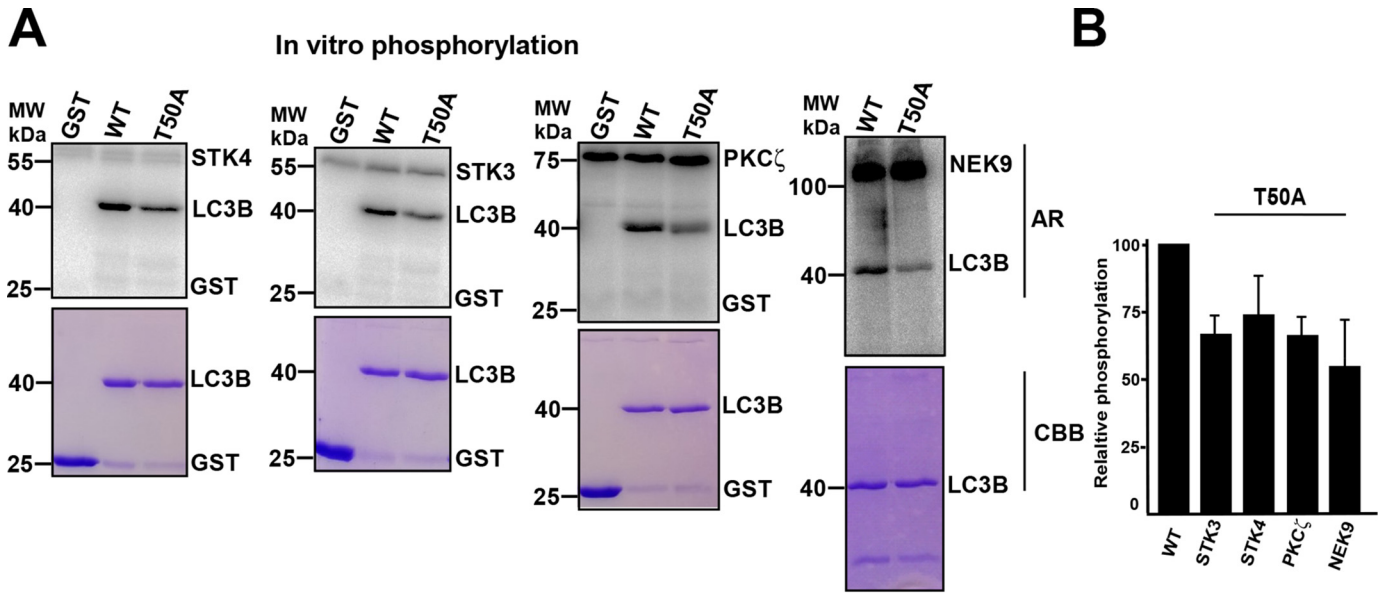

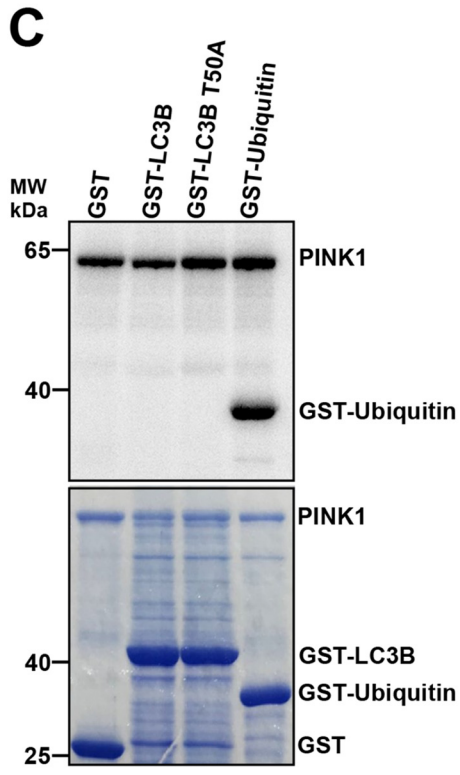

D

Sites of LC3B detected as phosphorylated by MS analyses following *in vitro* kinase assays

Kinase	Site	Xcorr	Intensity
NEK9	**T50**	**5.95**	**1.52E+08**
NEK9	T6	2.7	3.00E+07
NEK9	T29	6.06	9.07E+06
NEK9	S124	2.37	5.12E+06
NEK9	S87/S90	4.7/3.53	1.96E+06
NEK9	T12	5.31	1.21E+06
STK4	**T50**	**5.98**	**1.55E+08**
STK4	S3/T6	3.17/2.83	3.99E+07
STK4	T29	6.34	1.64E+07
STK4	S124	2.57	1.11E+07
STK4	S87/S90/S92	4.17/4.33/2.62	4.54E+06
STK4	T12	6.52	1.52E+06
STK3	T6	2.66	1.27E+07
STK3	**T50**	**5.9**	**1.25E+07**
STK3	T29	5.37	9.51E+06
STK3	T12	6.35	9.37E+05
STK3	S87	3	7.74E+04
PKCζ	T12	6.2	1.48E+06
PKCζ	T29	5.05	1.05E+06
PKCζ	**T50**	**3.49**	**3.49E+05**

Figure 4. NEK9, PKCζ, and STK3/4 phosphorylate LC3B *in vitro*. *A*, *in vitro* kinase assay. GST-tagged LC3B or LC3B T50A was incubated with the indicated kinases in the presence of [γ-^{32}P]ATP. Of note, FLAG–NEK9 was purified from HEK293 cells, and the other kinases were obtained from commercial vendors. Incorporation of radioactive-labeled phosphate was detected by AR, and immobilized GST or GST-tagged proteins were visualized by CBB staining. *B*, relative phosphorylation of LC3B WT/T50A normalized to the autophosphorylation of the kinase. Values are mean ± S.E. with quantifications of STK4/NEK9 ($n = 3$) and STK3/PKCζ ($n = 3$). *C*, *in vitro* kinase assay with PINK1 as the serine-threonine kinase and GST–LC3B and GST–ubiquitin as substrates. *D*, identification of phosphosites by MS following *in vitro* kinase assay with NEK9, STK4, STK3, and PKCζ.

Phospho-mimicking Thr-50 mutant of LC3B inhibits LIR–LDS binding

Phosphorylation of LC3B at Thr-50 by STK3/4 has been reported to be crucial for the fusion of the autophagosome with the lysosome (28). The potent ability of NEK9 and the STK3/4 kinases to phosphorylate Thr-50 *in vitro* prompted us to investigate further the biochemical consequences. Thr-50 is located close to Arg-10 in the N-terminal arm of LC3B, which forms part of the LDS (Fig. 5*A*). The Arg-10 residue is involved in electrostatic interactions with several LIR-containing proteins, including the Asp-336 residue at position −2 of the p62 LIR (Fig. 5*A*) (41). Phosphorylation of Thr-50 may impose a steric

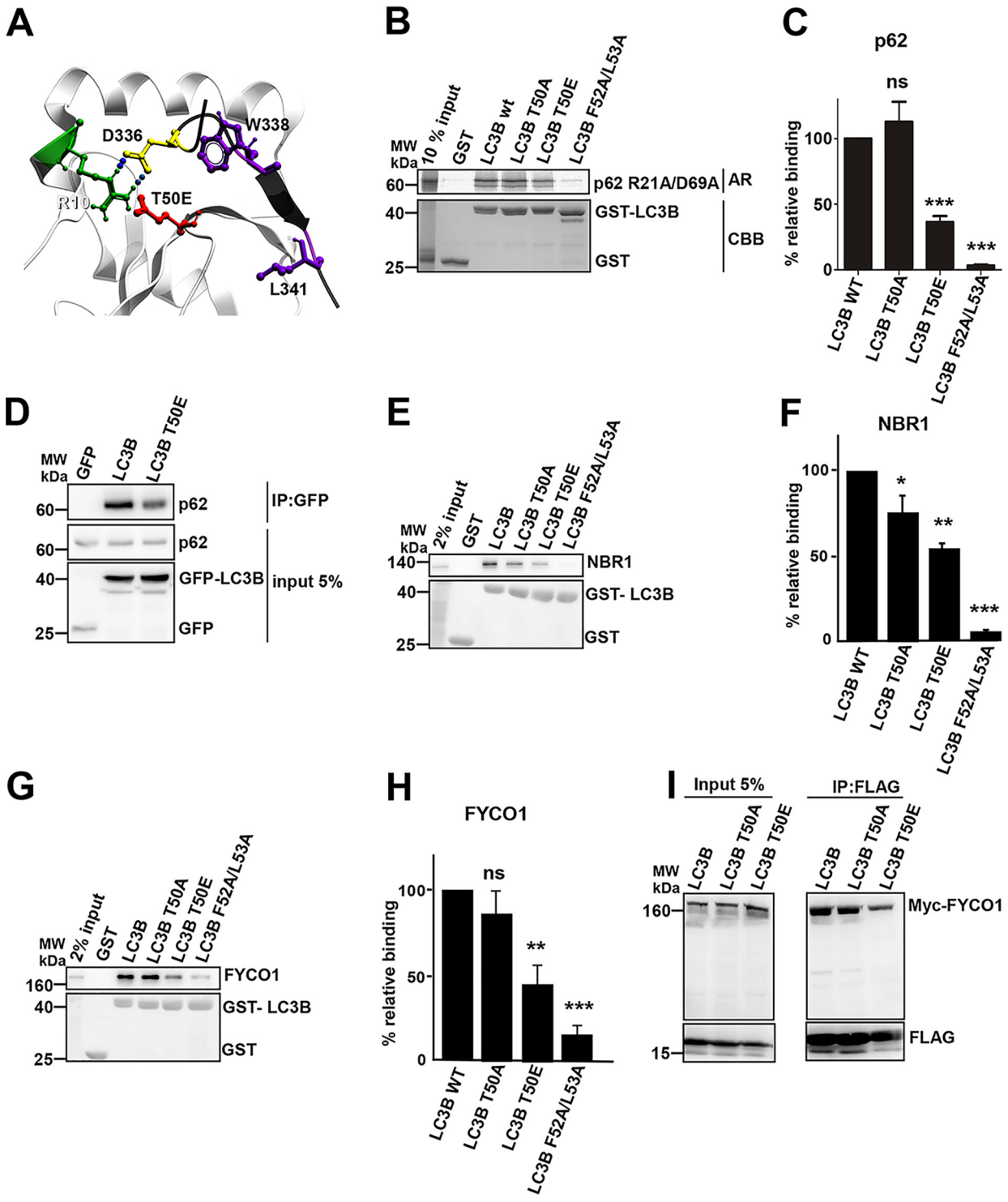

Figure 5. Phospho-mimicking T50E mutant of LC3B inhibits LIR–LDS interactions. *A*, structure of LC3B and p62 (Protein Data Bank code 2ZJD) in which Thr-50 is substituted by glutamic acid (*E*). The p62–LIR peptide is shown with a *black* backbone. The core p62 LIR residues Trp-338 and Leu-341 (*both purple*) are shown docking into HP1 and HP2, respectively. The structure shows the side chain of Arg-10 (*green*) of LC3B interacting with Asp-336 (*yellow*) of p62. T50E (*red*) is very close to Arg-10. *B*, Myc-tagged p62 R21A/D69A (monomeric mutant) was translated *in vitro* and tested for binding to LC3B fused to GST with or without mutations at Thr-50 or the LDS of LC3B. Bound proteins were detected by AR and immobilized GST or GST-tagged proteins by CBB. *C*, quantification of p62 binding shown in *B*, based on three independent experiments. *D*, HEK293 cells were transiently transfected with the indicated GFP-tagged LC3B constructs. Cell lysates were immunoprecipitated (*IP*) with GFP antibodies, and endogenous p62 was analyzed by Western blotting. *E*, recombinant GST or GST LC3B with or without mutation of Thr-50 and LDS mutation were incubated with RIPA buffer cell lysate from HeLa cells. The bound endogenous NBR1 was detected by immunoblotting with NBR1 antibodies. *F*, quantification of NBR1 binding is shown in *E*, based on three independent experiments. *G*, recombinant GST or GST LC3B with or without mutation of Thr-50 and LDS mutation was incubated with RIPA buffer cell lysate from HeLa cells and bound endogenous FYCO1 detected by immunoblotting. *H*, quantification of binding affinity of endogenous FYCO1 based on three independent replicates. *I*, HEK293 cells were transiently transfected with myc-FYCO1 and FLAG–LC3B. Cell lysates were immunoprecipitated with anti-FLAG antibodies and analyzed by Western blotting. For the quantifications, values are mean ± S.E.; $n = 3$; *ns* is $p > 0.05$; *, $p \leq 0.05$; **, $p \leq 0.01$; and ***, $p \leq 0.001$; one-way ANOVA.

hindrance for LIR–LDS interactions where Arg-10 of LC3B is engaged in binding an acidic residue N-terminal to the core LIR, such as in p62. We tested this first for the p62–LC3B LIR–LDS interaction. We employed myc-p62 with a mutated PB1 domain, unable to form polymers (42). The phospho-mimicking T50E mutant of LC3B exhibited a 60% reduced binding to p62 compared with WT in an *in vitro* GST-pulldown assay. The LC3B F52A/L53A double mutant affecting both hydrophobic pockets (HP1 and -2) of the LDS completely lost binding to p62 (Fig. 5, *B* and *C*). Furthermore, endogenous p62 co-precipitated with GFP–LC3B from HeLa cell extracts bound with less affinity to LC3B T50E compared with WT LC3B (Fig. 5*D*). These results clearly show that introducing a phospho-mimicking T50E mutation in LC3B reduces its affinity for the cargo receptor p62. Next, the binding of LC3B T50E to the autophagy receptor NBR1 was analyzed. Whole-cell extracts from HeLa cells was subjected to pulldown assays with WT, T50A, T50E, or F52A/L53A mutants of GST–LC3B and bound endogenous NBR1 detected by immunoblotting with an NBR1 antibody. The phospho-mimicking T50E mutant showed a 45% reduction in binding with endogenous NBR1 compared with WT LC3B (Fig. 5, *E* and *F*).

Thr-50 is conserved in the LC3 subfamily of ATG8s, but not present in the GABARAP subfamily (Fig. S1*B*). The kinesin adaptor and Rab7 effector FYCO1 transports autophagosomes along microtubules in the plus-end direction and has a clear preference for binding to LC3A and -B (43). The LC3B T50E mutation strongly reduced binding to endogenous FYCO1 in GST-pulldown assays and also when co-immunoprecipitated with myc-FYCO1 expressed in HeLa cells (Fig. 5, *G–I*). It is important to note that both NBR1 and FYCO1 also displayed a slight reduction in binding with LC3B T50A, indicating that this substitution also affects LIR–LDS binding, albeit slightly.

The cysteine protease ATG4B is required for processing of LC3B before conjugation to phosphatidylethanolamine (PE) and for delipidation and recycling of LC3B (44). To test whether T50E would compromise efficient binding of ATG4B, we conducted a GST pulldown assay with translated *in vitro* ATG4B probed against GST–LC3B WT, T50A, T50E, and the LDS double mutant F52A/L53A. Importantly, ATG4B displayed less affinity for LC3B T50E than for WT LC3B (Fig. 6*A*). In GST-pulldown assays with endogenous ATG4B from HeLa cell lysates, LC3B T50E showed 74% reduction in binding with ATG4B compared with LC3B WT and very little binding to the LDS mutant (Fig. 6, *B* and *C*).

The efficient conjugation of LC3 to PE requires sequential interaction of LC3 with ATG3 and ATG7 (45, 46). To investigate whether the interaction of LC3B with ATG7 was affected by the T50E mutant, GST pulldown with endogenous ATG7 was done. The phospho-mimicking mutant LC3B T50E almost lost all binding to ATG7, whereas LC3B T50A and LC3B F52A/L53A (LDS) bound similarly to WT (Fig. 6, *D* and *E*).

ATG8s family proteins are essential both for efficient autophagosome biogenesis and fusion with lysosomes (13). The role of ATG8s in the fusion of autophagosomes with lysosomes has been shown via its interaction with syntaxin 17 (STX17) (47) and PLEKHM1 (48). Both STX17 and PLEKHM1 are known to interact with ATG8s via LIR motifs (47, 48). Consistent with the results obtained for interaction with the other LIR-containing ATG8 interactors tested here, LC3B T50E showed a strongly reduced binding affinity for STX17. Almost no binding of STX17 was seen for the LDS mutant LC3B F52A/L53A, and there was also reduced binding to LC3B T50A (Fig. 6, *F* and *G*).

Taken together all these results show that binding of LIR-containing protein to LC3B T50E is compromised. This can be explained by steric hindrance and charge repulsions occurring due to the close proximity of Thr-50 to the LDS. Phosphorylation of Thr-50 will most likely exaggerate the effects observed with T50E, having an even stronger impact on LIR–LDS interactions.

LC3B T50E phospho-mimicking mutant impairs selective autophagic flux of p62 and NBR1

To investigate the importance of the phosphorylation of LC3B on Thr-50, we established an LC3B knockout (KO) cell line to avoid the influence of endogenous LC3B. We employed the CRISPR/Cas9 system targeting exon 2 of the human *LC3B* gene on chromosome 16 to generate a Flp-In T-Rex HEK293 cell line lacking expression of LC3B (Fig. S3, *A* and *B*). The LC3B KO cells showed accumulation of the selective autophagy receptors p62/SQSTM1 and NBR1 compared with WT cells (Fig. 7, *A* and *B*). In contrast to the effect of LC3B KO on the selective autophagic degradation of p62 and NBR1, we did not find any difference in bulk autophagy measured by the LDH sequestration assay (Fig. S3*C*) (49). The result is in line with earlier publications where KD of LC3s affects p62 degradation but not bulk autophagy measured by LDH sequestration assay (50, 51). To avoid any overexpression artifacts, we employed stable reconstitution of the LC3B KO cells by use of the Flp-In system under the control of a tetracycline-inducible promoter. LC3B KO cell lines with reintroduced Myc–LC3B WT, Myc–LC3B T50A, Myc–LC3B T50E, and the LDS mutant F52A/L53A were established (Fig. 7*C*). Reduced lipidation was observed for T50E, and no lipidation was seen for the LDS mutant. An increase in lipidation was seen for T50A as expected because LDS binding cannot be negatively regulated by phosphorylation (Fig. 7*C*). The reconstitution of LC3B KO cells with Myc–LC3B WT restored the autophagic flux as indicated by a reduced level of p62 and NBR1. Interestingly, the reconstitution of Myc–LC3B T50E and Myc–LC3B F52A/L53A led to a strongly-reduced autophagic degradation of p62 and NBR1 (Fig. 7*D*). To further investigate the autophagic turnover of the LC3B T50A and T50E mutants in the KO cells, we reintroduced mCherry–YFP–LC3B WT and mutants. The mCherry–YFP tag allows for monitoring entry into acidic structures such as the lysosome because YFP fluorescence is rapidly lost in acidic structures, leaving only mCherry as a functioning fluorophore (52). First, we quantitated the amount of LC3B-containing puncta (indicative of autophagosomes) per cell. We scored the ability of the different cell lines to produce LC3B puncta during starvation. Although more than 90% of LC3B WT ($n = 550$) and T50A cells ($n = 710$) contained LC3B puncta, the T50E cell line ($n = 680$) exhibited puncta in 75% of the cells. We had to exclude the LC3B F52A/L53A cell line because, as expected, only a few cells produced LC3B puncta.

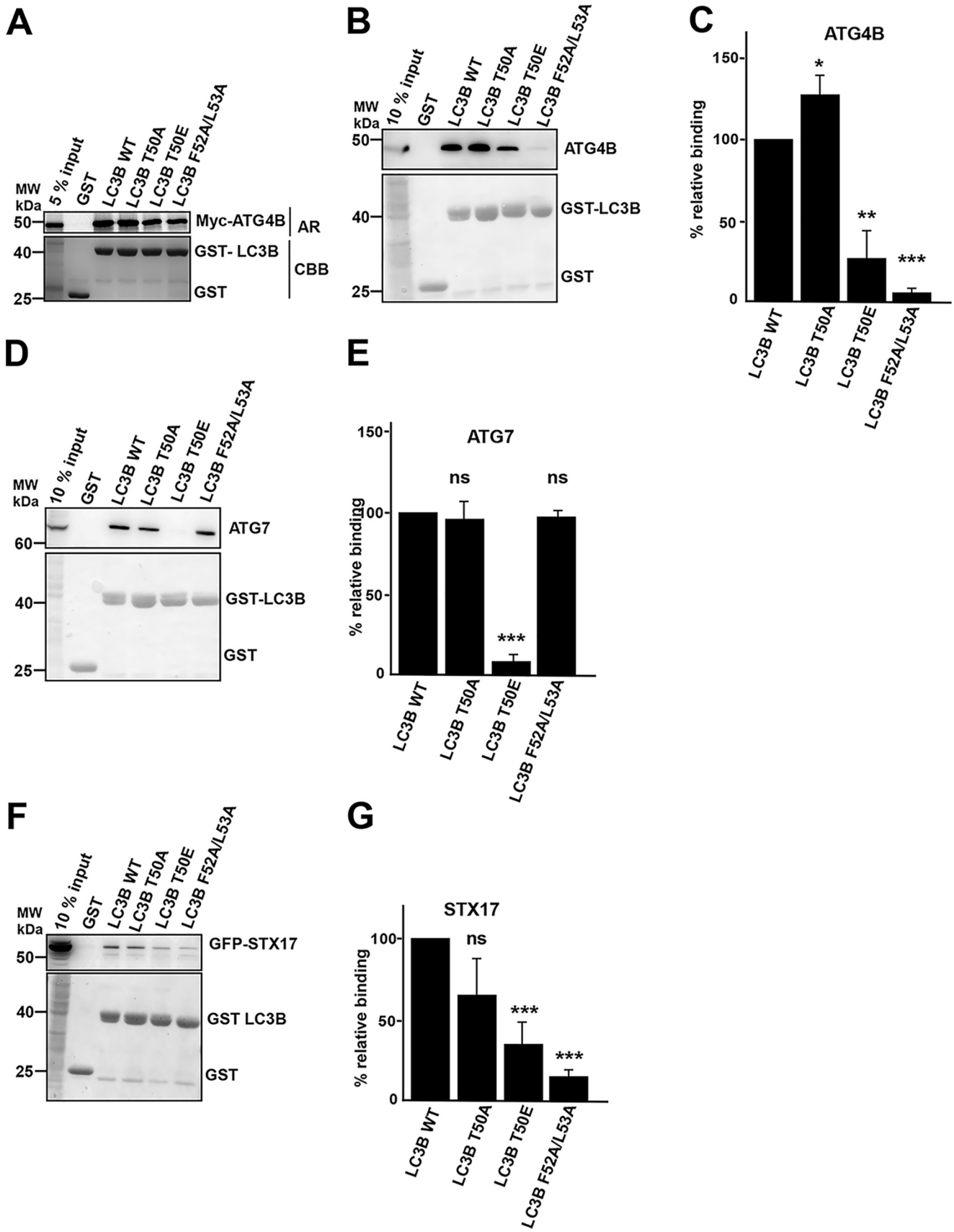
A
MW kDa
5 % input
GST
LC3B WT
LC3B T50A
LC3B T50E
LC3B F52A/L53A
50
40
25
Myc-ATG4B
AR
GST- LC3B
CBB
GST
B
MW kDa
10 % input
GST
LC3B WT
LC3B T50A
LC3B T50E
LC3B F52A/L53A
50
40
25
ATG4B
GST-LC3B
GST
C
ATG4B
% relative binding
150
100
50
0
*
**
***
LC3B WT
LC3B T50A
LC3B T50E
LC3B F52A/L53A
D
MW kDa
10 % input
GST
LC3B WT
LC3B T50A
LC3B T50E
LC3B F52A/L53A
60
40
25
ATG7
GST-LC3B
GST
E
ATG7
% relative binding
150
100
50
0
ns
ns
***
LC3B WT
LC3B T50A
LC3B T50E
LC3B F52A/L53A
F
MW kDa
10 % input
GST
LC3B WT
LC3B T50A
LC3B T50E
LC3B F52A/L53A
50
40
25
GFP-STX17
GST LC3B
GST
G
STX17
% relative binding
100
50
0
ns
***
***
LC3B WT
LC3B T50A
LC3B T50E
LC3B F52A/L53A

Only by actively searching for LC3B puncta–containing cells were we able to identify cells with LC3B puncta (less than 15%; $n = 220$) (Fig. 7*E*). Next, we focused on the cells containing LC3B puncta in WT, T50A, and T50E cell lines. Looking at the number of puncta per cell volume, we found slightly fewer LC3B puncta in the T50A cell line when compared with LC3B WT (Fig. 7*F*) and more so during starvation (Fig. 7*G*). LC3B T50E–expressing cells displayed a strongly reduced amount of LC3B-containing puncta, both when grown in full medium and when starved in Hanks' medium (Fig. 7, *F* and *G*). For each construct, we determined the ratio of red-only to yellow puncta. When grown in full medium, LC3B T50E displayed a slightly-reduced fraction of red only puncta compared with LC3B WT and T50A, indicating that T50E-positive puncta do not have a higher turnover rate (Fig. 7*H*). In conclusion, the lower total amount of puncta in the T50E cell line is caused by a reduced ability of LC3B T50E to become lipidated. Notably, the lower fraction of red-only puncta under basal conditions may indicate that not only formation but also maturation of LC3B-positive puncta is affected by the T50E mutation (Fig. 7*H*). However, when starved, there was no statistically significant difference in the fraction of red-only puncta between the cells (Fig. 7*H*).

Selective autophagic degradation of p62 and NBR1 is negatively regulated by NEK9 and positively regulated by STK3/4, whereas PKCζ has no effect

Our results from *in vitro* kinase assays and binding studies with a number of autophagy-related proteins clearly begged the question whether selective autophagy could be regulated via phosphorylation of LC3B Thr-50. To address this, we knocked down the individual kinases STK3, STK4, PKCζ, and NEK9 and measured the turnover of p62 in full medium (Fig. 8, *A–H*). Knockdown of NEK9 led to a decreased level of p62 in full medium (Fig. 8, *A–C*). To further validate the NEK9 KD data, we generated HeLa NEK9 KO cells using CRISPR/Cas9 (Fig. S3, *D* and *E*). In HeLa NEK9 KO cells we also observed increased autophagic degradation of p62 and NBR1 as well as increased LC3B lipidation in full medium (Fig. 8*D*). In contrast to NEK9 KD or KO, KD of STK3 and -4 showed increased p62 levels and LC3B lipidation levels indicating inhibition of autophagy (Fig. 8*E*). To further support our siRNA-mediated KD data, we generated CRISPR/Cas9 STK3/4 double KO cells (Fig. S4, *A–C*). In STK3/4 double KO cells, we also found both increased p62 levels and decreased lipidation of LC3B (Fig. 8, *F–G*). The accumulation of lipidated LC3B indicates an inhibition of maturation of LC3B-positive autophagosomes. These results are in line with a previous study where it was shown that STK3/4 KO inhibits autophagosome–lysosome fusion (28). In contrast to NEK9 KD and KO and STK3/4 KD and KO, we observed no effect on selective degradation of p62 by PKCζ KD suggesting PKCζ might not be involved in regulation of selective autophagy (Fig. 8*H*). To determine whether regulation of selective autophagy via NEK9 and STK3/4 is mediated via the Thr-50 site of LC3B, we knocked down NEK9 and STK3/STK4 in HEK293 LC3B KO cells reconstituted with WT Myc–LC3B, Myc–LC3B T50A, and Myc–LC3B T50E mutant. KD of NEK9 in HEK293 LC3B KO cells reconstituted with WT Myc–LC3B led to a reduction in p62 levels, although this did not occur in LC3B KO cells reconstituted with LC3B T50A or LC3B T50E (Fig. 8*I*). In contrast to KD of NEK9, the KD of STK3 and -4 resulted in an increased accumulation of p62 in LC3B KO cells reconstituted with either WT LC3B, LC3B T50A, or LC3B T50E (Fig. 8*J*). This suggests a more general inhibition of autophagy that is not mediated through the Thr-50 site of LC3B. In conclusion, our results suggest that NEK9 inhibits autophagic degradation of p62 via phosphorylation of LC3B at the Thr-50 site, whereas STK3/4 positively regulates autophagy independent of the Thr-50 site.

Discussion

The hippo kinases have previously been reported to phosphorylate LC3B at Thr-50 (28). Here, we show that *in vitro* NEK9 phosphorylates this residue very efficiently, whereas PKCζ is also able to phosphorylate this residue, but with far lower efficiency. Furthermore, we mapped an atypical C-type LIR motif mediating binding to LC3C and GABARAP in STK3, a GABARAP-preferring LIR motif overlapping with the AGC kinase–docking motif in PKCζ, and a C-terminal LIR motif in NEK9 mediating efficient binding to both LC3 and GABARAP subfamily members of the ATG8 family proteins. Knockdown and KO experiments showed that NEK9 acts to inhibit the selective autophagic degradation of p62 and NBR1. This inhibition is mediated via phosphorylation of Thr-50 in LC3B. Our reasoning is partly based on our findings that the LC3B T50E phospho-mimicking mutant impaired selective autophagic flux by inhibiting LIR–LDS binding to a number of autophagy-related proteins. These include the selective autophagy receptors p62 and NBR1, the basal autophagy proteins important for conjugation and delipidation of LC3B ATG7 and ATG4B, FYCO1 involved in microtubule-dependent transport of autophagosomes and lysosomes, and the SNARE STX17 implicated both early and late in the process of autophagosome formation and maturation. We also base the conclusion on NEK9 inhibiting autophagy of p62 on the results of siRNA-mediated knockdown of NEK9 and reconstitution of LC3B KO cells with WT and T50A and T50E mutants of LC3B.

Figure 6. T50E mutant of LC3B inhibits LIR–LDS interactions with ATG4B, ATG7, and syntaxin-17 (STX17). *A*, Myc-tagged ATG4B was translated *in vitro* in the presence of [^{35}S]methionine and subjected to GST pulldown assays with recombinant GST–LC3B WT, T50A, T50E, and the LDS double mutant F52A/L53A. Bound proteins were detected by AR and immobilized GST or GST-tagged proteins by CBB staining. *B*, GST pulldown assays using RIPA buffer cell lysate from HeLa cells with recombinant GST–LC3B WT, T50A, T50E, and the LDS double mutant F52A/L53A. The bound endogenous ATG4B was detected by immunoblotting. *C*, quantification of binding affinity of endogenous ATG4B based on three biological replicates. *D*, HeLa cell lysates were used in GST pulldown assays as in *B* except that ATG7 binding was analyzed by immunoblotting of the bound fraction. *E*, quantification of ATG7 binding affinity from three independent experiments. *F*, HeLa cells were transfected with EGFP–Syntaxin 17 (GFP–STX17), and cells were lysed with RIPA buffer. The cell lysate was incubated with recombinant GST or GST LC3B with or without the indicated mutations. Bound GFP–STX17 was detected by Western blotting with EGFP antibody. *G*, quantification of binding affinity of GFP–STX17 based on three biological replicates. For the quantifications values are mean ± S.E.; $n = 3$; *ns*, $p > 0.05$; *, $p \leq 0.05$; **, $p \leq 0.01$; and ***, $p \leq 0.001$; one-way ANOVA.

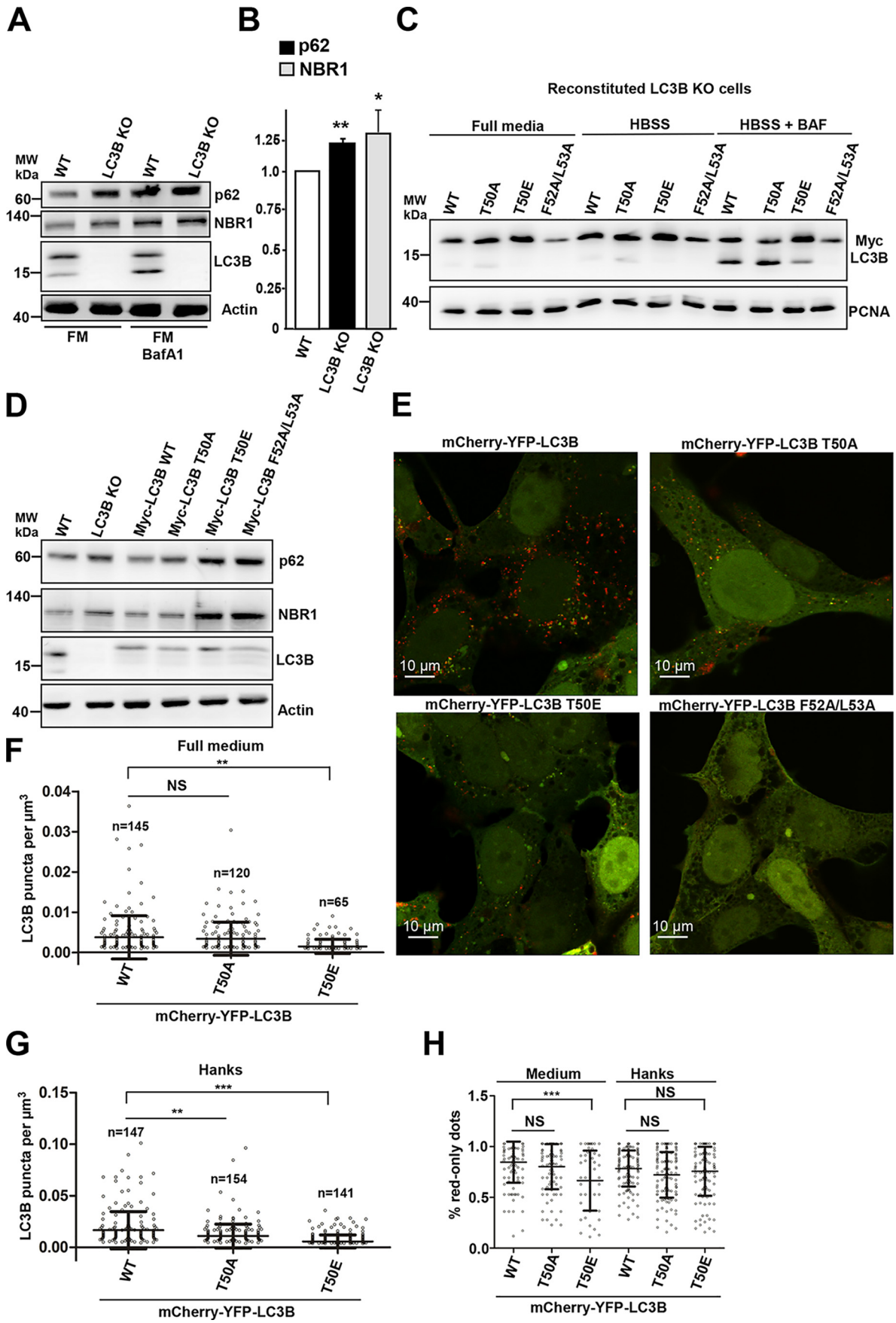
A
MW kDa
WT
LC3B KO
WT
LC3B KO
60
140
15
40
p62
NBR1
LC3B
Actin
FM
FM BafA1
B
p62
NBR1
1.25
1.0
0.75
0.5
0.25
0
**
*
WT
LC3B KO
LC3B KO
C
Reconstituted LC3B KO cells
Full media
HBSS
HBSS + BAF
MW kDa
WT
T50A
T50E
F52A/L53A
15
40
Myc LC3B
PCNA
D
MW kDa
WT
LC3B KO
Myc-LC3B WT
Myc-LC3B T50A
Myc-LC3B T50E
Myc-LC3B F52A/L53A
60
140
15
40
p62
NBR1
LC3B
Actin
E
mCherry-YFP-LC3B
mCherry-YFP-LC3B T50A
mCherry-YFP-LC3B T50E
mCherry-YFP-LC3B F52A/L53A
10 μm
F
Full medium
**
NS
LC3B puncta per μm3
0.04
0.03
0.02
0.01
0.00
n=145
n=120
n=65
WT
T50A
T50E
mCherry-YFP-LC3B
G
Hanks
***
**
LC3B puncta per μm3
0.15
0.10
0.05
0.00
n=147
n=154
n=141
WT
T50A
T50E
mCherry-YFP-LC3B
H
Medium
Hanks
***
NS
NS
NS
% red-only dots
1.5
1.0
0.5
0.0
WT
T50A
T50E
WT
T50A
T50E
mCherry-YFP-LC3B

STK4 has previously been shown to bind to ATG8s *in vitro*. However, the binding appeared weaker than the binding of STK3 to the ATG8s (19). We also observed this difference in binding *in vitro* between STK3 and -4. Interestingly, knockdown of STK3 was recently shown to have the most dramatic effect on autophagy measured as an increased basal level of p62 and increased level of lipidated LC3B (28). Our findings support these earlier published results about STK3/4 positively regulating autophagy. However, a difference is that we found that the positive effect STK3/4 has on degradation of p62 does not depend on phosphorylation of the LC3B Thr-50 site. Interestingly, ERK8/MAPK15 binds to LC3B via an LIR motif, but it does not phosphorylate LC3B itself and is reported to positively-regulate autophagy (53). Hence, in future studies it would be interesting to explore the functional importance of the STK3 LIR motif and to identify all the substrates of STK3/4 involved in regulating autophagy. In addition to influencing autophagy, STK3 was also shown to stimulate xenophagy by enhancing the clearance of bacteria via phosphorylation of the LC3B Thr-50 site (28). The xenophagy receptor NDP52 has been shown to rely on binding to LC3C (17, 36). Here, we show that STK3 has a preference for binding to GABARAP and LC3C, and we identified a C-type LIR (MVI) in STK3. Consistent with our finding that the phospho-mimicking mutant T50E negatively affects its LIR–LDS-mediated interactions, the LC3C T56A/T56E mutants significantly reduced its interaction with NDP52 (Fig. S4, *D* and *E*). Clearly, this link to the regulation of xenophagy warrants further studies.

Interestingly, the CLIR of STK3 and surrounding residues has been identified as a nuclear export signal (54). Furthermore, the STK3 substrate MOB1 has been shown to bind to STK3 dependent on several phosphorylated threonines, with Thr-364 (next to the LIR) being the most crucial for this binding (55), indicating a possible competition for this site in STK3.

Previously, PKCζ has only been indirectly implicated in the phosphorylation of LC3B (27). However, it has long been known that PKCζ/ι binds p62 (42) and thereby might co-localize with LC3B *in vivo*. The atypical PKCι, which is very similar to PKCζ, has been shown to negatively regulate autophagy via PIK3CA/AKT–mTOR signaling (25). Our study showed that PKCζ does not regulate degradation of p62 by autophagy. However, we mapped a functional LIR motif in PKCζ that overlaps completely with the AGC kinase docking motif, a hydrophobic motif known to mediate PKCζ interaction with its activating kinase, PDK1 (56). This hydrophobic motif is essential for the activation of PKCζ by PDK1. In future studies, it will be interesting to investigate different conditions where interactions mediated by these overlapping motifs might influence the roles of PKCζ, or PKCι, in regulation of autophagy and other cellular processes.

Except for the pioneering study of Behrends *et al.* (19), NEK9 has not been implicated in autophagy processes or the regulation of autophagy before. In the Behrends *et al.* paper (19), NEK9 was scored among the positive regulators of autophagosome formation based on a reduced amount of LC3-positive puncta formed upon siRNA-mediated KD of NEK9. We also see reduced lipidated LC3B upon KO of NEK9, but this can also be interpreted as an increased turnover (Fig. 8*D*). This would then be consistent with our findings of an inhibitory role of NEK9 on selective autophagy. We found that NEK9 interacted strongly with all ATG8s compared with PKCζ, which showed preferential binding toward GABARAPs.

We show that the Thr-50 phospho-mimicking mutant displays a strongly reduced binding to several autophagy-related proteins. A phosphorylatable residue in the LDS of LC3B is intriguing as it might function as a dynamic "switch" governing which proteins bind to LC3B. Regulation of LDS binding by phosphorylation/dephosphorylation might be executed at a certain stage(s) of autophagosome formation and maturation adding another regulatory layer. An intriguing idea is that LC3B on a fully-matured autophagosome becomes phosphorylated at Thr-50. This causes canonical LIR-binding proteins to dissociate, leaving ATG4B to delipidate LC3B from the autophagosome. Such a model might also explain why we observed less II-form of LC3B T50E. If LC3B T50E is unable to bind effectively to cargo receptors such as p62 on the inside of the phagophore, LC3B might be exposed for ATG4B-mediated delipidation. This way LC3B T50E is delipidated, removed from the autophagosome before maturation, and thus is no longer sequestered inside the autophagosome, hence the lower amount of LC3B-II. Importantly, phosphorylation is assumed to have a greater effect on all the interactions and functions of LC3B, due to the more negatively charged and bulky phosphate compared with our phosphor-mimicking glutamic acid. One of the limitations of using a phospho-mimicking T50E mutant is that it is mimicking a constitutively phosphorylated state. So, the phospho-mimicking T50E mutant behaves as a constitutively dominant-negative on LIR–LDS interactions that might affect both autophagosome formation and autophagosome–lysosomal fusion. Such an effect is supported by our results

Figure 7. Phospho-mimicking T50E mutation inhibits autophagic flux of the selective autophagy receptors p62 and NBR1. *A*, Western blot analysis of p62 and NBR1 levels in HEK293 WT and HEK293 LC3B KO cells. Actin was probed as a loading control. *B*, quantification of p62 and NBR1 levels in WT and LC3B KO cells from three biological replicates. *C*, Western blottings of Myc–LC3B in cell lysates from HEK293 LC3B KO cells reconstituted with Myc–LC3B-WT, -LC3B T50A, -LC3B T50E, and Myc–LC3B F52A/L53A and grown in full medium only, or in full media first and then incubated for 4 h in HBSS, or for 4 h in HBSS with bafilomycin A1 (*HBSS + BAF*). The blot was developed using anti-Myc antibodies, and proliferating cell nuclear antigen (*PCNA*) was used as the loading control. *D*, Western blottings of p62 and NBR1 in cell lysates from HEK293 WT and LC3B KO cells reconstituted with Myc–LC3B–WT, -LC3B T50A, -LC3B T50E, and Myc–LC3B F52A/L53A and grown in full medium. Actin was used as a loading control. *E–H,* under basal conditions (full medium) both formation and maturation of LC3B positive puncta (autophagosomes) are negatively affected by the T50E mutation. *E*, representative confocal fluorescence microscopy images of starving cells expressing the different mCherry–YFP–LC3B constructs used in *F–H*. The indicated LC3B cell lines expressing mCherry–YFP–LC3B WT, -LC3B T50A, -LC3B T50E, and mCherry–YFP–LC3B F52A/L53A were induced with tetracycline (1 μg/ml) for 24 h and grown in full medium or buffered Hanks' balanced salt solution for 2 h after which the cells were fixed and analyzed by confocal microscopy. Individual cells were marked, and LC3B-containing puncta were plotted as a function of cell volume for cells grown in full medium (*F*) or in Hanks' balanced salt solution for the final 2 h (*G*). The total number of cells scored is indicated *above* the plots. Note only cells positive for LC3B puncta are included. Results represent three independent experiments (*H*). The ratio of red-only to yellow puncta from the experiment shown in *F* and *G* was analyzed for the different cell lines. Mean ± S.E. of three independent experiments: *NS*, $p > 0.05$; *, $p \leq 0.05$; **, $p \leq 0.01$; ***, $p \leq 0.001$. One-way ANOVA was followed by the Tukey multiple comparison test.

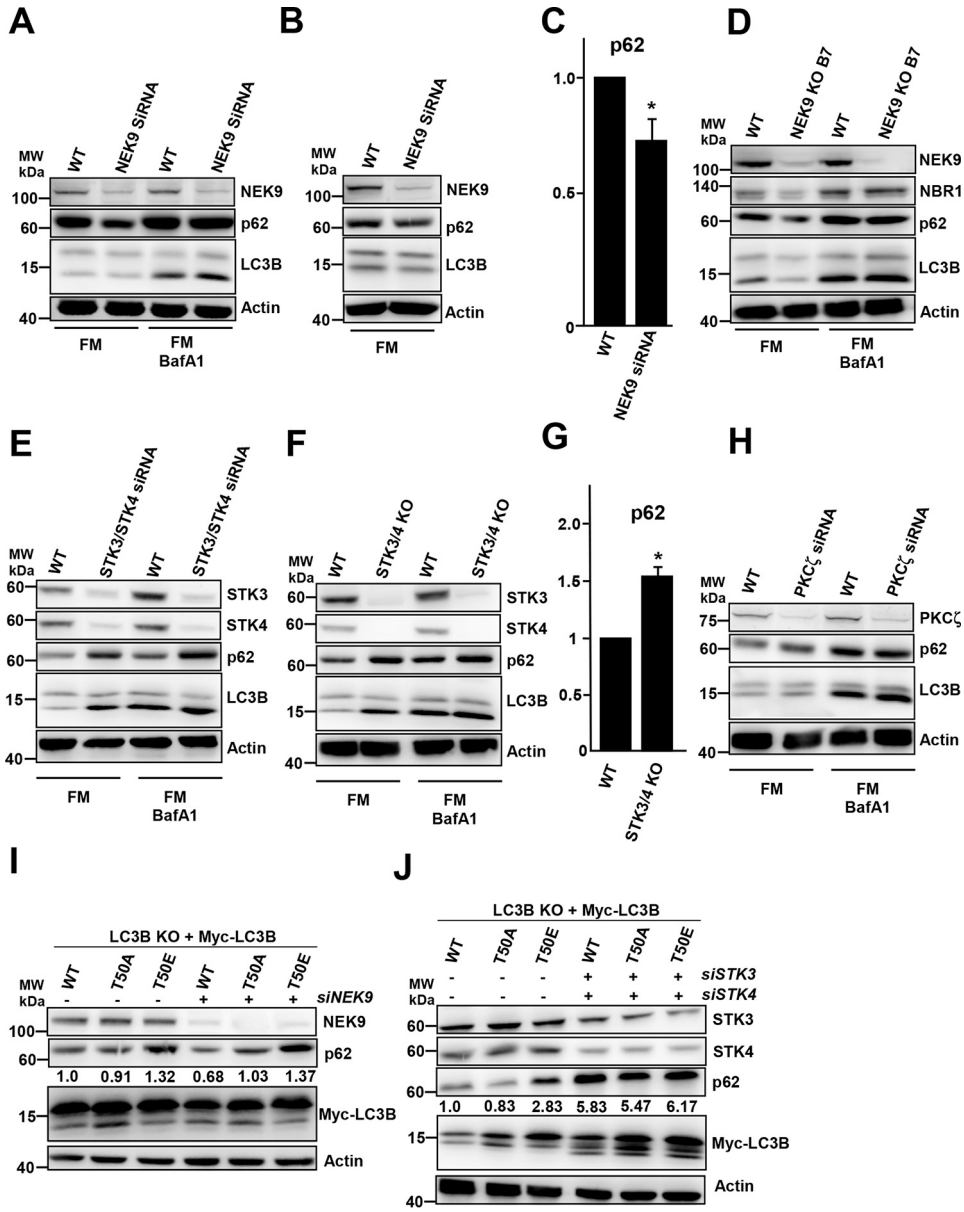

Figure 8. NEK9 negatively regulates the selective autophagic degradation of p62 and NBR1; STK3/4 positively regulates autophagy, and PKCζ has no effect. *A*, and *B*, Western blot analysis of p62 in HeLa cells with control siRNA and NEK9 SmartPool siRNA. Actin was used as loading control. *C*, quantification of p62 levels following siRNA-mediated knockdown of NEK9 in full medium based on three biological replicates. Values are mean ± S.E.; $n = 3$; *, $p < 0.05$; one-way ANOVA. *D*, Western blottings of cell extracts from HeLa WT and HeLa NEK9 KO cells with antibodies against NEK9, NBR1, p62, and LC3B with β-actin as loading control. *E*, Western blot analysis of p62 in HeLa cells with control siRNA and STK3/4 SmartPool siRNA. Actin was used as loading control. *F*, Western blottings of cells extracts from HeLa WT and STK3/4 KO cells. *G*, quantification of p62 levels in HeLa WT cells and STK3/4 KO cells based on three biological replicates. Values are mean ± S.E.; $n = 3$; *, $p < 0.05$; one-way ANOVA. *H*, Western blotting showing level of p62 in HeLa cells treated with control siRNA and PKCζ SmartPool siRNA. *I*, Western blot analysis of p62 level from cell extracts harvested after transfection with control siRNA and NEK9 siRNA on HEK293 LC3B KO cells reconstituted with Myc–LC3B WT, Myc–LC3B T50A, and Myc–LC3B T50E. *J*, Western blot analysis of p62 level from cell extract harvested after treatment with control siRNA and STK3/4 siRNA on HEK293 LC3B KO reconstituted with Myc–LC3B WT, Myc–LC3B T50A, and Myc–LC3B T50E. *I* and *J*, relative band intensities of p62 (ratio of p62 signal to the actin loading control) with the value obtained from WT LC3B in KO cells with control siRNA set to 1.0 are shown *below* the p62 blots. Values for representative experiments performed twice are shown.

where the selective autophagic flux is reduced as well as the formation of autophagosomes (fewer puncta).

Interestingly, during starvation, the LC3B T50A cell line was also less able to make puncta than LC3B WT (Fig. 7, *E* and *G*). This may indicate that phosphorylation of Thr-50 is important for autophagosome formation. Hence, puncta formation is inhibited, and this might be more evident during the fast protein turnover occurring during starvation. We saw no consistent difference between the Myc-tagged versions of LC3B WT and T50A neither in the amount of p62 nor the band pattern of LC3B. Furthermore, there was no difference between LC3B WT and T50A in the fraction of red-only puncta between full medium and starvation. This indicates that the slightly-negative effect of T50A is occurring during autophagosome formation.

The reduced ability of LC3B T50E to become lipidated may seem surprising when considering the reported positive effect on the fusion of autophagosomes and lysosomes (28). However,

Table 1
Gateway cloning vectors

Plasmid	Description	Source
pENTR1A, -2B, and -3C	Gateway entry vectors	Invitrogen
pDest 3×FLAG	Mammalian triple Flag-tagged expression vector, CMV	62
pDestEGFP-C1	Mammalian EGFP-tagged expression vector, CMV	42
pDest15	Bacterial GST-tagged expression vector, T7 promoter	Invitrogen
pDestYFP–Flp-In	Mammalian Flp-In expression vector, Tet-inducible, CMV	30

Table 2
Gateway entry clones

Plasmid	Source
pENTR–STK3	This study
pENTR–STK4	This study
pDONOR223–NEK9	Addgene plasmid no. 23459
pENTR–FYCO1	63
pENTR–NBR1	42
pENTR–p62	42
pENTR–ATG4B	64
pENTR–GABARAP	52
pENTR–GABARAPL1	52
pENTR–GABARAPL2	52
pENTR–LC3A	52
pENTR–LC3B	52
pENTR–LC3C	52
pENTR–STK3(1–357)	This study
pENTR–STK3(1–411)	This study
pENTR–STK3(1–404)	This study
pENTR–STK3(F402A/K405A)	This study
pENTR–STK3(323–491)	This study
pENTR–STK3 Δ405–411	This study
pENTR–STK3 D146N	This study
pENTR–STK3 MVI365–367AAA	This study
pENTR–STK4 D149N	This study
pDONOR223–NEK9 D179N	This study
pENTR–GABARAP Y49A	52
pENTR–LC3C F58A	This study
pENTR–LC3B T50A	This study
pENTR–LC3B T50E	This study
pENTR–LC3B F52A/L53A	This study
pENTR–NBR1 D50R ΔCC	42
pDONOR223–NEK9 W718A/I721A	This study
pDONOR223–NEK9 Y845A/L848A	This study
pDONOR223–NEK9 W967A/L970A	This study
pENTR–ATG7	This study
pENTR–PKCζ	This study
pENTR–PKCζ F37A/L40A	This study
pENTR–PKCζ F252A/I255A	This study
pENTR–PKCζ W434A_L454A	This study
pENTR–PKCζ W575A/I578A	This study
pENTR–LC3C T56A	This study
pENTR–LC3C T56E	This study

neither our *in vitro* binding data nor *in vivo* data support a pro-autophagic role of the phosphorylation of Thr-50. There are, however, important differences between the studies. First, the study by Wilkinson *et al.* (28) is based on the transient overexpression of LC3B harboring Thr-50 mutations. Second, they did not use an LC3B knockout cell line. Our cell lines mimic global phosphorylation, which might retard a dynamic process depending on only a fractional pool of phosphorylated LC3B at any one time. Our data support that LC3B lipidation is impaired and that interactions of LC3B with effector proteins on the inner or outer surface of the phagophore/autophagosome are strongly reduced. Furthermore, roles not directly related to autophagy have been reported for LC3B (57), such as the regulation of endocytic pathways (58), and the Rho-signaling pathway (59). How the phosphorylation of Thr-50 affects these pathways *in vivo* was not addressed. Because these interactions are reported to be LIR-mediated, it is likely that the phosphorylation also affects these interactors. Recently, acetylation of residues in the LDS was shown to have a drastic effect on LC3B causing LC3B to be unable to produce puncta (29). We show that the phospho-mimicking T50E mutant also strongly affects LC3B function strengthening the notion of a potent regulation of the LDS by PTMs. Both acetylation and phosphorylation sites in the LDS region are conserved within the LC3 subfamily of ATG8 proteins.

Recent KD and KO studies of ATG8 family members show that GABARAPs are critical facilitators of autophagic flux (51, 60, 61). LC3 family proteins are not required for nonselective, bulk degradation of cytosolic proteins, whereas GABARAPs are required (51). A similar conclusion was reached for some forms of selective autophagy based on triple KOs of LC3 or GABARAP subfamily members (60, 61). However, we observed that cells only KO for LC3B displayed impaired turnover of p62 and NBR1, although the effect was not very strong. The T50E mutant had a stronger effect, most likely because it also has a dominant-negative effect. More studies will be required to determine the relative contributions of the different ATG8 family members to different forms of selective autophagy. We have also just begun to elucidate how PTMs may regulate LIR–LDS interactions and the effects mediated on different steps of the autophagy pathway.

Experimental procedures

Plasmids

The Gateway entry clones used in this study are listed in Tables 1–3. QuikChange site-directed mutagenesis kit (Stratagene) was used to create desired point mutation, which was verified by DNA sequencing (BigDye Sequencing kits, Applied Biosystems). For a generation of Gateway destination plasmid, the Gateway LR and BP recombination kit from Invitrogen was used.

Cell culture

HEK293 cells were cultured in DMEM (Sigma, D6046) supplemented with 10% fetal bovine serum (Biochrom, S0615) and 1% streptomycin/penicillin (Sigma, P4333). HEK293 FlpIn T-Rex cell lines were cultured in high-glucose DMEM (Sigma, D5671). For amino acid and serum starvation, Hanks' balanced salt solution was used (Sigma, H9269).

Generation of stable cell lines

LC3B KO HEK293 FlpIn T-Rex cells were used to make stable LC3 mutant cell lines. The mCherry–YFP or Myc-tagged LC3B WT, LC3B phospho-mimicking mutant (T50E), T50A, and LC3B LDS mutants (F52A–Leu-53) were cloned into pcDNA 3.1 FRT/TO plasmid. The generation of a stable cell line was made in accordance with the manufacturer's instructions (Invitrogen, V6520-20). Briefly, the different mutants of LC3B expressed from pcDNA 3.1 FRT/TO plasmids were transfected into LC3B KO cells. Following 48 h of transfection, colonies of cells with the gene of interest integrated into the FRT site were selected with 150 ng/ml hygromycin (Calbi-

Table 3
Gateway expression clones

Plasmid	Source
pDestmCherry YFP–Flp-In–LC3B	This study
pDestmCherry YFP–Flp-In–LC3B T50A	This study
pDestmCherry YFP–Flp-In–LC3B T50E	This study
pDestmCherry YFP–Flp-In–LC3B F52A/L53A	This study
pDestMyc–Flp-In–LC3B	This study
pDestMyc–Flp-In–LC3B T50A	This study
pDestMyc–Flp-In–LC3B T50E	This study
pDestMyc–Flp-In–LC3B F52A/L53A	This study
pDestMyc ATG4B	64
pDestMyc ATG7	This study
pDestMyc NBR1 D50R ΔCC1	65
pDestMyc NEK9	This study
pDestMyc NEK9 W718A/I721A	This study
pDestMyc NEK9 Y845A/L848A	This study
pDestMyc NEK9 W967A/L970A	This study
pDest3XFlag–NEK9 D179N	This study
pDestMyc–STK3 1–357	This study
pDestMyc–STK3 1–411	This study
pDestMyc–STK3 1–404	This study
pDestMyc–STK3 F402A/K405A	This study
pDestMyc–STK3 323–491	This study
pDestMyc–STK3 Δ405–411	This study
pDestMyc–STK3 D146N	This study
pDestMyc–STK3 MVI365–367AAA	This study
pENTR–STK4 D149N	This study
pENTR–STK3 D146N	This study
pDest15–GABARAP	52
pDest15–GABARAPL1	52
pDest15–GABARAPL2	52
pDest15–LC3A	52
pDest15–LC3B	52
pDest15–LC3C	52
pDestMyc–PKCζ	This study
pDestMyc–PKCζ F37A/L40A	This study
pDestMyc–PKCζ F252A/I255A	This study
pDestMyc–PKCζ W434A_L454A	This study
pDestMyc–PKCζ W575A/I578A	This study
pDestMyc–LC3C T56A	This study
pDestMyc–LC3C T56E	This study

ochem, 400051). The expression of the gene was induced with 1 μg/ml tetracycline for 24 h.

CRISPR/Cas9

To construct the LC3B/NEK9/STK3/STK4 specific CRISPR/Cas9 vectors the sense and antisense oligonucleotides encoding the selection guide sequences were annealed and then inserted into plasmid pSpCas9(BB)-2A-Puro (PX459). For a generation of CRISPR/Cas9 KO cells, ~30,000 of HEK293 Flp-In T-Rex cells were seeded into 24-well plates and then 500 ng of plasmid PX459 per well were transfected using Metafectene Pro (Biontex, T040). The clonal selection was achieved by puromycin treatment 24 h after transfection for 48–72 h. Later, single cells were sorted into 96-well plates via FACS sorting. The clones were allowed to grow for 7–10 days, and each clone was screened for KO by both Western blotting and DNA sequencing of PCR products amplified from the targeted region in the genome.

Peptide arrays

Peptides were synthesized on cellulose membranes using a MultiPep automated peptide synthesizer (INTAVIS Bioanalytical Instruments AG, Cologne, Germany), as described previously. Membranes were blocked using 5% nonfat dry milk in TBS containing 0.1% Tween 20. The membrane was probed by overlaying with 1 μg/ml of either GST–GABARAP for 2 h at room temperature. Membranes were washed three times in TBS containing 0.1% Tween 20. Bound protein was detected with horseradish peroxidase-conjugated anti-GST antibody (GE Healthcare, RPN1236).

Antibodies and reagents

The following antibodies were used: rabbit anti-LC3B (Novus, NB100-2220); mouse anti-p62 (BD Biosciences, 610833); rabbit anti-CALCOCO2 (Abcam, AB68588); mouse anti-NBR1 (Santa Cruz Biotechnology, sc-130380); rabbit anti-GFP (Abcam, AB290); rabbit anti-actin (Sigma, A2066); mouse anti-FLAG (Sigma, F3165); rabbit anti-ATG7 (Cell Signaling, 8558); rabbit anti-ATG4B (Santa Cruz Biotechnology, sc-130968); mouse anti-Myc (Cell Signaling, 2276); rabbit anti-STK3 (Abcam, ab52641); rabbit anti-STK4 (Cell Signaling, 3682); rabbit anti-PKCζ (Cell Signaling, 9372); rabbit anti-NEK9 (Abcam, ab138488); rabbit anti-FYCO1 (Sigma, HPA0355526); horseradish peroxidase-conjugated goat anti-mouse (BD Biosciences, 554002); and anti-rabbit (BD Biosciences, 554021) secondary antibodies. Other reagents used were bafilomycin A1 (Santa Cruz Biotechnology, sc-201550) and [^{35}S]methionine (PerkinElmer Life Sciences, NEG709A500UC).

siRNA transfection

The target small interfering RNAs (siRNAs) were transfected into cells by reverse transfection. The transfection was carried out using Lipofectamine RNAiMax(Invitrogen 13778) protocol. The siRNAs were used at final concentration of 20 nM, and experiments were performed 48 h post-transfection. The following validated predesign target siRNAs purchased from Dharmacon were used in our study: ON-TARGETplus SMARTpool human STK3 (L-004874-00-0005); ON-TARGETplus SMARTpool human STK4 (L-004157-00-00056789); siGENOME SMARTpool human NEK9 (M-004869-01-0005); and siGENOME SMARTpool human PKCζ (M-003526-03-0005).

Protein purification and GST affinity isolation experiments

GST-tagged proteins were expressed in *E. coli* BL21 (DE3). GST-(Atg8-family proteins) fusion proteins were purified on GSH-Sepharose 4 Fast Flow beads (GE Healthcare, 17513201) followed by washing with NET-N buffer (100 mM NaCl, 1 mM EDTA, 0.5% Nonidet P-40 (Sigma, 74385), 50 mM Tris-HCl, pH 8) supplemented with cOmplete Mini EDTA-free protease inhibitor mixture tablets (Roche Applied Science, 118361-70001). GST-tagged proteins were eluted with 50 mM Tris, pH 8, 200 mM NaCl, 5 mM L-GSH reduced (Sigma, G425). GST-affinity isolation assays were performed with ^{35}S-labeled proteins co-transcribed and translated using the TNT Coupled Reticulocyte Lysate System (Promega, L4610) as described previously. For quantifications, gels were vacuum-dried, and ^{35}S-labeled proteins were detected on a Fujifilm bioimaging analyzer BAS-5000 (Fujifilm, Tokyo, Japan).

Kinase assay

Kinase assays were performed in a 25-μl final volume, containing 50 ng of recombinant active kinases, 1–2 μg of substrate proteins, 60 μM ATP, 2 μCi/sample of [γ-^{32}P]ATP in 35.5 mM Tris-HCl, pH 7.5, 10 mM MgCl, 0.5 mM EGTA, pH 8.0, 0.1 mM $CaCl_2$. The kinase reaction was stopped by the addition of 5×

SDS-loading buffer followed by boiling for 5 min. Commercially-available His-tagged kinases were used unless otherwise stated (PKCζ: Millipore, 14-525M; STK3: Millipore, 14-524; STK4: Millipore, 14-624). FLAG-tagged kinases were obtained by transient expression of HEK cells with WT or KD kinases, and after immunoprecipitation of the FLAG-tag, different amounts of eluted kinase were run in the kinase assay as above. The expression of kinases from cells was verified with Western blotting. Proteins were resolved by SDS-PAGE and stained with Coomassie Blue. Gels were vacuum-dried and ^{32}P-labeled proteins detected on a Fujifilm bioimaging analyzer BAS-5000 (Fujifilm, Tokyo, Japan).

For identification of phosphorylation sites, *in vitro*-kinase assays were performed as stated above in the absence of radioactive ATP. SDS-PAGE-resolved proteins were analyzed by mass spectrometry to identify phosphorylation sites.

Mass spectrometry

In-gel chymotrypsin digestion was performed before analysis by HPLC-tandem MS (HPLC-MS/MS). Gel pieces were subjected to in-gel reduction, alkylation, and digestion using 6 ng/μl chymotrypsin (V1062; Promega). OMIX C18 tips (Varian) were used for sample cleanup and concentration. Peptide mixtures containing 0.1% formic acid were loaded onto a Thermo Fisher Scientific EASY-nLC1200 system. Samples were injected to a trap column (Acclaim PepMap 75 μm × 2 cm, C18, 3 μm, 100 Å; Thermo Fisher Scientific) for desalting before elution to the separation column (EASY-Spray column, C18, 2 μm, 100 Å, 50 μm, 50 cm; Thermo Fisher Scientific). Peptides were fractionated using a 4–40% gradient of increasing amounts of 80% acetonitrile in water over 60 min at a flow rate of 300 nl/min. The mobile phases contained 0.1% formic acid. Separated peptides were analyzed using an Orbitrap Fusion Lumos mass spectrometer. The mass spectrometer was operated in a data-dependent mode with the precursor scan in the orbitrap over the range m/z 350–1500. The most intense ions were selected for ETD or CID fragmentation using 3 s between each master scan. Dynamic exclusion was set to 8 s. The Orbitrap AGC target was set to 4E5 with a maximum injection time of 50 ms. The MS2 scans in the Ion Trap or orbitrap was set to 1E4 with a dynamic injection time. Precursor ions with charge 3+ in the m/z range 350–650 and 4+ or 5+ ions in the m/z range 350–900 were fragmented with ETD. All ions with charge of 6+ or higher were also fragmented using ETD. The rest of the precursor ions were fragmented using CID. Protein identification and PTM mapping was done using the Proteome Discoverer 2.4 software (Thermo Fisher Scientific) using the ptmRS module (>75%). Peak lists generated in Proteome Discoverer were searched against the UniProt *Homo sapiens* proteome (April, 2019; 73,645 sequences) using the built-in Sequest HT search engine. Search parameters were as follows: enzyme, chymotrypsin (full); maximum missed cleavage, 2; precursor mass tolerance, 10 ppm; fragment mass tolerance, 0.02 Da (Orbitrap); 0.6 Da (Ion Trap); fixed modifications: carbamidomethyl (C); dynamic modifications: oxidation (M), phospho (ST), acetyl (protein N-terminal), Met-loss (protein N-terminal), Met-loss + acetyl (protein N-terminal); threshold score Xcorr >2.0; no. of peptides >2. The MS proteomics data have been deposited to the ProteomeXchange Consortium via the PRIDE (66) partner repository with the dataset identifier PXD016681.

LDH sequestration assay

The autophagic sequestration assay was performed by measuring the activity of autophagosomal lactate dehydrogenase (49). For LDH sequestration assay, cells were seeded in 6-well plates either in complete medium or incubated in HBSS in the presence of 200 nM of bafilomycin for 4 h. The cells were then harvested by using Accumax. Later, harvested cells were washed with solution containing 10% sucrose and 1% BSA. The washing steps were followed by resuspension in solution containing 10% sucrose and 0.2% BSA. These resuspended cells were electro-disrupted by a single high-voltage pulse at 2 kV/cm using an electrode chamber. The disrupted cells were diluted in 400 μl of phosphate-buffered sucrose (100 mM sodium phosphate, 2 mM DTT, 2 mM EDTA and 1.75% sucrose, pH 7.5). Then, 600 μl of the disrupted cells are transferred to new tubes that are further diluted with 900 μl of resuspension buffer (RSB; 50 mM sodium phosphate, 1 mM EDTA, 1 mM DTT) containing 0.5% BSA and 0.01% Tween 20. Finally, the tubes were centrifuged for 30 min at 20,000 × *g*. The pellet and the total cell lysate (200 μl) were freeze-thawed at −80 °C. The pellets were resuspended in 500 μl of RSB containing 1% Triton X-405, and the total cell lysates were further diluted with 200 μl of RSB/2% Triton X-405. The short centrifugation at 21,000 × *g* for 5 min was carried out to remove cell debris. The LDH activity was measured in a multianalyzer (MaxMat PL-II, Erba Diagnostics) by using an LDH assay kit (RM LADH0126V, Erba Diagnostics). The net LDH sequestration value was calculated by measuring the amount of LDH sedimented with cell pellets relative to the amount in total cell lysate. The rate of LDH sequestration (%/h) was calculated by dividing net value with incubation time.

Western blotting and immunoprecipitation experiments

For Western blotting experiments, cells were washed in PBS (137 mM NaCl, 2.7 mM KCl, 4.3 mM Na_2HPO_4, 1.47 mM KH_2PO_4, pH 7.4) followed by lysis directly in SDS-PAGE loading buffer (2% SDS, 10% glycerol, 50 mM Tris-HCl, pH 6.8) and boiled for 10 min. Protein concentration was measured followed by addition of bromphenol blue (0.1%) and DTT (100 mM). Samples (20 μg) were run on 10–16% gradient or 10% SDS-polyacrylamide gels and blotted on Hybond nitrocellulose membranes (GE Healthcare, 10600003) followed by Ponceau S staining. Blocking was performed in 5% nonfat dry milk in PBS/Tween 20 (0.1%). The primary antibody was diluted in PBS/Tween 20 containing 5% nonfat dry milk, and incubation was performed overnight at 4 °C. Secondary antibody incubation was performed at room temperature for 1 h in PBS/Tween 20 containing 5% nonfat dry milk. Membranes were washed three times prior to the addition of secondary antibody and development using LAS-300 (Fujifilm, Tokyo, Japan). Immunoprecipitations were performed by use of either GFP-Trap–agarose in accordance with the manufacturer's instructions (Chromotek, gta-20) or anti-FLAG affinity gel (Sigma, A2220). For immunoprecipitations of FLAG-tagged proteins, cells were grown and

transfected with 2 μg of the plasmid in 6-cm dishes, and after 24 h the cells were washed and lysed in RIPA buffer followed by centrifugation to remove cell debris. After the removal of input control, the lysate was incubated with FLAG affinity gel overnight. The gel was washed five times in RIPA buffer and analyzed by Western blotting. For GST pulldowns using cell extracts, FLAG-tagged kinases were eluted by addition of the FLAG peptide (100 μg/ml) (Sigma, F3290), and the eluate was evenly divided to tubes containing GST-tagged ATG8s prepared as described above.

Bioinformatics and statistics

Data in all figures are shown as means ± S.E. from at least three independent experiments unless otherwise stated. Statistical significance was evaluated with one-way ANOVA followed by the Tukey multiple comparison test performed in PRISM (Graphpad) (ns is $p > 0.05$; *, $p \leq 0.05$; **, $p \leq 0.01$; and ***, $p \leq 0.001$).

Author contributions—B. K. S., M. S. R., Y. P. A., J.-A. B., K. B. L., E. A. A., T. L., and T. J. data curation; B. K. S., M. S. R., K. B. L., E. A. A., E. S., and T. L. validation; B. K. S., M. S. R., Y. P. A., J.-A. B., E. A. A., E. S., and T. L. investigation; B. K. S., M. S. R., Y. P. A., and K. B. L. visualization; B. K. S., M. S. R., Y. P. A., J.-A. B., K. B. L., E. A. A., and T. L. methodology; B. K. S., M. S. R., E. A. A., E. S., T. L., and T. J. writing-original draft; B. K. S., M. S. R., Y. P. A., J.-A. B., K. B. L., E. A. A., E. S., T. L., and T. J. writing-review and editing; M. S. R. and T. J. formal analysis; E. S., T. L., and T. J. supervision; T. L. and T. J. conceptualization; T. J. funding acquisition; T. J. project administration.

Acknowledgments—We thank Nikolai Engedal for help with establishing the LDH sequestration assay. We are grateful to the proteomics and imaging core facilities at the Faculty of Health Sciences, The Arctic University of Norway, for valuable assistance.

References

1. Mizushima, N., and Komatsu, M. (2011) Autophagy: renovation of cells and tissues. *Cell* **147,** 728–741 CrossRef Medline
2. Wen, X., and Klionsky, D. J. (2016) An overview of macroautophagy in yeast. *J. Mol. Biol.* **428,** 1681–1699 CrossRef Medline
3. Parzych, K. R., and Klionsky, D. J. (2014) An overview of autophagy: morphology, mechanism, and regulation. *Antioxid. Redox Signal.* **20,** 460–473 CrossRef Medline
4. Rogov, V., Dötsch, V., Johansen, T., and Kirkin, V. (2014) Interactions between autophagy receptors and ubiquitin-like proteins form the molecular basis for selective autophagy. *Mol. Cell* **53,** 167–178 CrossRef Medline
5. Lamark, T., Svenning, S., and Johansen, T. (2017) Regulation of selective autophagy: the p62/SQSTM1 paradigm. *Essays Biochem.* **61,** 609–624 CrossRef Medline
6. Katsuragi, Y., Ichimura, Y., and Komatsu, M. (2015) p62/SQSTM1 functions as a signaling hub and an autophagy adaptor. *FEBS J.* **282,** 4672–4678 CrossRef Medline
7. Johansen, T., and Lamark, T. (2011) Selective autophagy mediated by autophagic adapter proteins. *Autophagy* **7,** 279–296 CrossRef Medline
8. Shpilka, T., Weidberg, H., Pietrokovski, S., and Elazar, Z. (2011) Atg8: an autophagy-related ubiquitin-like protein family. *Genome Biol.* **12,** 226 CrossRef Medline
9. Tanida, I., Sou, Y. S., Ezaki, J., Minematsu-Ikeguchi, N., Ueno, T., and Kominami, E. (2004) HsAtg4B/HsApg4B/autophagin-1 cleaves the carboxyl termini of three human Atg8 homologues and delipidates microtubule-associated protein light chain 3- and GABAA receptor-associated protein-phospholipid conjugates. *J. Biol. Chem.* **279,** 36268–36276 CrossRef Medline
10. Taherbhoy, A. M., Tait, S. W., Kaiser, S. E., Williams, A. H., Deng, A., Nourse, A., Hammel, M., Kurinov, I., Rock, C. O., Green, D. R., and Schulman, B. A. (2011) Atg8 transfer from Atg7 to Atg3: a distinctive E1-E2 architecture and mechanism in the autophagy pathway. *Mol. Cell* **44,** 451–461 CrossRef Medline
11. Yang, Z., and Klionsky, D. J. (2009) An overview of the molecular mechanism of autophagy. *Curr. Top. Microbiol. Immunol.* **335,** 1–32 CrossRef Medline
12. Xie, Z., Nair, U., and Klionsky, D. J. (2008) Atg8 controls phagophore expansion during autophagosome formation. *Mol. Biol. Cell* **19,** 3290–3298 CrossRef Medline
13. Weidberg, H., Shvets, E., Shpilka, T., Shimron, F., Shinder, V., and Elazar, Z. (2010) LC3 and GATE-16/GABARAP subfamilies are both essential yet act differently in autophagosome biogenesis. *EMBO J.* **29,** 1792–1802 CrossRef Medline
14. Kabeya, Y., Mizushima, N., Ueno, T., Yamamoto, A., Kirisako, T., Noda, T., Kominami, E., Ohsumi, Y., and Yoshimori, T. (2000) LC3, a mammalian homologue of yeast Apg8p, is localized in autophagosome membranes after processing. *EMBO J.* **19,** 5720–5728 CrossRef Medline
15. Birgisdottir, Å. B., Lamark, T., and Johansen, T. (2013) The LIR motif–crucial for selective autophagy. *J. Cell Sci.* **126,** 3237–3247 CrossRef Medline
16. Noda, N. N., Kumeta, H., Nakatogawa, H., Satoo, K., Adachi, W., Ishii, J., Fujioka, Y., Ohsumi, Y., and Inagaki, F. (2008) Structural basis of target recognition by Atg8/LC3 during selective autophagy. *Genes Cells* **13,** 1211–1218 CrossRef Medline
17. von Muhlinen, N., Akutsu, M., Ravenhill, B. J., Foeglein, Á., Bloor, S., Rutherford, T. J., Freund, S. M., Komander, D., and Randow, F. (2013) An essential role for the ATG8 ortholog LC3C in antibacterial autophagy. *Autophagy* **9,** 784–786 CrossRef Medline
18. Jung, C. H., Ro, S. H., Cao, J., Otto, N. M., and Kim, D. H. (2010) mTOR regulation of autophagy. *FEBS Lett.* **584,** 1287–1295 CrossRef Medline
19. Behrends, C., Sowa, M. E., Gygi, S. P., and Harper, J. W. (2010) Network organization of the human autophagy system. *Nature* **466,** 68–76 CrossRef Medline
20. Fry, A. M., O'Regan, L., Sabir, S. R., and Bayliss, R. (2012) Cell cycle regulation by the NEK family of protein kinases. *J. Cell Sci.* **125,** 4423–4433 CrossRef Medline
21. Piccolo, S., Dupont, S., and Cordenonsi, M. (2014) The biology of YAP/TAZ: hippo signaling and beyond. *Physiol. Rev.* **94,** 1287–1312 CrossRef Medline
22. Nehme, N. T., Schmid, J. P., Debeurme, F., André-Schmutz, I., Lim, A., Nitschke, P., Rieux-Laucat, F., Lutz, P., Picard, C., Mahlaoui, N., Fischer, A., and de Saint Basile, G. (2012) MST1 mutations in autosomal recessive primary immunodeficiency characterized by defective naive T-cell survival. *Blood* **119,** 3458–3468 CrossRef Medline
23. Abdollahpour, H., Appaswamy, G., Kotlarz, D., Diestelhorst, J., Beier, R., Schäffer, A. A., Gertz, E. M., Schambach, A., Kreipe, H. H., Pfeifer, D., Engelhardt, K. R., Rezaei, N., Grimbacher, B., Lohrmann, S., Sherkat, R., and Klein, C. (2012) The phenotype of human STK4 deficiency. *Blood* **119,** 3450–3457 CrossRef Medline
24. Maejima, Y., Kyoi, S., Zhai, P., Liu, T., Li, H., Ivessa, A., Sciarretta, S., Del Re, D. P., Zablocki, D. K., Hsu, C. P., Lim, D. S., Isobe, M., and Sadoshima, J. (2013) Mst1 inhibits autophagy by promoting the interaction between Beclin1 and Bcl-2. *Nat. Med.* **19,** 1478–1488 CrossRef Medline
25. Qu, L., Li, G., Xia, D., Hongdu, B., Xu, C., Lin, X., and Chen, Y. (2016) PRKCI negatively regulates autophagy via PIK3CA/AKT-MTOR signaling. *Biochem. Biophys. Res. Commun.* **470,** 306–312 CrossRef Medline
26. Xie, Y., Kang, R., Sun, X., Zhong, M., Huang, J., Klionsky, D. J., and Tang, D. (2015) Posttranslational modification of autophagy-related proteins in macroautophagy. *Autophagy* **11,** 28–45 CrossRef Medline
27. Jiang, H., Cheng, D., Liu, W., Peng, J., and Feng, J. (2010) Protein kinase C inhibits autophagy and phosphorylates LC3. *Biochem. Biophys. Res. Commun.* **395,** 471–476 CrossRef Medline
28. Wilkinson, D. S., Jariwala, J. S., Anderson, E., Mitra, K., Meisenhelder, J., Chang, J. T., Ideker, T., Hunter, T., Nizet, V., Dillin, A., and Hansen, M.

(2015) Phosphorylation of LC3 by the Hippo kinases STK3/STK4 is essential for autophagy. *Mol. Cell* **57,** 55–68 CrossRef Medline

29. Huang, R., Xu, Y., Wan, W., Shou, X., Qian, J., You, Z., Liu, B., Chang, C., Zhou, T., Lippincott-Schwartz, J., and Liu, W. (2015) Deacetylation of nuclear LC3 drives autophagy initiation under starvation. *Mol. Cell* **57,** 456–466 CrossRef Medline
30. Alemu, E. A., Lamark, T., Torgersen, K. M., Birgisdottir, A. B., Larsen, K. B., Jain, A., Olsvik, H., Øvervatn, A., Kirkin, V., and Johansen, T. (2012) ATG8 family proteins act as scaffolds for assembly of the ULK complex: sequence requirements for lc3-interacting region (LIR) motifs. *J. Biol. Chem.* **287,** 39275–39290 CrossRef Medline
31. Kraft, C., Kijanska, M., Kalie, E., Siergiejuk, E., Lee, S. S., Semplicio, G., Stoffel, I., Brezovich, A., Verma, M., Hansmann, I., Ammerer, G., Hofmann, K., Tooze, S., and Peter, M. (2012) Binding of the Atg1/ULK1 kinase to the ubiquitin-like protein Atg8 regulates autophagy. *EMBO J.* **31,** 3691–3703 CrossRef Medline
32. Cameron, A. J., Escribano, C., Saurin, A. T., Kostelecky, B., and Parker, P. J. (2009) PKC maturation is promoted by nucleotide pocket occupation independently of intrinsic kinase activity. *Nat. Struct. Mol. Biol.* **16,** 624–630 CrossRef Medline
33. Liu, H. S., Jan, M. S., Chou, C. K., Chen, P. H., and Ke, N. J. (1999) Is green fluorescent protein toxic to the living cells? *Biochem. Biophys. Res. Commun.* **260,** 712–717 CrossRef Medline
34. Ni, L., Li, S., Yu, J., Min, J., Brautigam, C. A., Tomchick, D. R., Pan, D., and Luo, X. (2013) Structural basis for autoactivation of human Mst2 kinase and its regulation by RASSF5. *Structure* **21,** 1757–1768 CrossRef Medline
35. Avruch, J., Zhou, D., Fitamant, J., Bardeesy, N., Mou, F., and Barrufet, L. R. (2012) Protein kinases of the Hippo pathway: regulation and substrates. *Semin. Cell Dev. Biol.* **23,** 770–784 CrossRef Medline
36. von Muhlinen, N., Akutsu, M., Ravenhill, B. J., Foeglein, Á., Bloor, S., Rutherford, T. J., Freund, S. M., Komander, D., and Randow, F. (2012) LC3C, bound selectively by a noncanonical LIR motif in NDP52, is required for antibacterial autophagy. *Mol. Cell* **48,** 329–342 CrossRef Medline
37. Johansen, T., Birgisdottir, Å. B., Huber, J., Kniss, A., Dötsch, V., Kirkin, V., and Rogov, V. V. (2017) Methods for studying interactions between Atg8/LC3/GABARAP and LIR-containing proteins. *Methods Enzymol.* **587,** 143–169 CrossRef Medline
38. Balendran, A., Biondi, R. M., Cheung, P. C., Casamayor, A., Deak, M., and Alessi, D. R. (2000) A 3-phosphoinositide-dependent protein kinase-1 (PDK1) docking site is required for the phosphorylation of protein kinase Cζ (PKCζ) and PKC-related kinase 2 by PDK1. *J. Biol. Chem.* **275,** 20806–20813 CrossRef Medline
39. Kalvari, I., Tsompanis, S., Mulakkal, N. C., Osgood, R., Johansen, T., Nezis, I. P., and Promponas, V. J. (2014) iLIR: A web resource for prediction of Atg8-family interacting proteins. *Autophagy* **10,** 913–925 CrossRef Medline
40. Wirth, M., Zhang, W., Razi, M., Nyoni, L., Joshi, D., O'Reilly, N., Johansen, T., Tooze, S. A., and Mouilleron, S. (2019) Molecular determinants regulating selective binding of autophagy adapters and receptors to ATG8 proteins. *Nat. Commun.* **10,** 2055 CrossRef Medline
41. Ichimura, Y., Kumanomidou, T., Sou, Y. S., Mizushima, T., Ezaki, J., Ueno, T., Kominami, E., Yamane, T., Tanaka, K., and Komatsu, M. (2008) Structural basis for sorting mechanism of p62 in selective autophagy. *J. Biol. Chem.* **283,** 22847–22857 CrossRef Medline
42. Lamark, T., Perander, M., Øutzen, H., Kristiansen, K., Øvervatn, Michaelsen, E., Bjørkøy, G., and Johansen, T. (2003) Interaction codes within the family of mammalian Phox and Bem1p domain-containing proteins. *J. Biol. Chem.* **278,** 34568–34581 CrossRef Medline
43. Olsvik, H. L., Lamark, T., Takagi, K., Larsen, K. B., Evjen, G., Øvervatn, A., Mizushima, T., and Johansen, T. (2015) FYCO1 contains a C-terminally extended, LC3A/B-preferring LC3-interacting region (LIR) motif required for efficient maturation of autophagosomes during basal autophagy. *J. Biol. Chem.* **290,** 29361–29374 CrossRef Medline
44. Nair, U., Yen, W. L., Mari, M., Cao, Y., Xie, Z., Baba, M., Reggiori, F., and Klionsky, D. J. (2012) A role for Atg8-PE deconjugation in autophagosome biogenesis. *Autophagy* **8,** 780–793 CrossRef Medline
45. Ichimura, Y., Kirisako, T., Takao, T., Satomi, Y., Shimonishi, Y., Ishihara, N., Mizushima, N., Tanida, I., Kominami, E., Ohsumi, M., Noda, T., and Ohsumi, Y. (2000) A ubiquitin-like system mediates protein lipidation. *Nature* **408,** 488–492 CrossRef Medline
46. Nakatogawa, H., Ichimura, Y., and Ohsumi, Y. (2007) Atg8, a ubiquitin-like protein required for autophagosome formation, mediates membrane tethering and hemifusion. *Cell* **130,** 165–178 CrossRef Medline
47. Kumar, S., Jain, A., Farzam, F., Jia, J., Gu, Y., Choi, S. W., Mudd, M. H., Claude-Taupin, A., Wester, M. J., Lidke, K. A., Rusten, T. E., and Deretic, V. (2018) Mechanism of Stx17 recruitment to autophagosomes via IRGM and mammalian Atg8 proteins. *J. Cell Biol.* **217,** 997–1013 CrossRef Medline
48. McEwan, D. G., Popovic, D., Gubas, A., Terawaki, S., Suzuki, H., Stadel, D., Coxon, F. P., Miranda de Stegmann, D., Bhogaraju, S., Maddi, K., Kirchof, A., Gatti, E., Helfrich, M. H., Wakatsuki, S., *et al.* (2015) PLEKHM1 Regulates Autophagosome-Lysosome fusion through HOPS complex and LC3/GABARAP proteins. *Mol. Cell* **57,** 39–54 CrossRef Medline
49. Luhr, M., Szalai, P., and Engedal, N. (2018) The lactate dehydrogenase sequestration assay–a simple and reliable method to determine bulk autophagic sequestration activity in mammalian cells. *J. Vis. Exp.* 2018, **137,** CrossRef Medline
50. Maruyama, Y., Sou, Y. S., Kageyama, S., Takahashi, T., Ueno, T., Tanaka, K., Komatsu, M., and Ichimura, Y. (2014) LC3B is indispensable for selective autophagy of p62 but not basal autophagy. *Biochem. Biophys. Res. Commun.* **446,** 309–315 CrossRef Medline
51. Szalai, P., Hagen, L. K., Saetre, F., Luhr, M., Sponheim, M., Øverbye, A., Mills, I. G., Seglen, P. O., and Engedal, N. (2015) Autophagic bulk sequestration of cytosolic cargo is independent of LC3, but requires GABARAPs. *Exp. Cell Res.* **333,** 21–38 CrossRef Medline
52. Pankiv, S., Clausen, T. H., Lamark, T., Brech, A., Bruun, J. A., Outzen, H., Øvervatn, A., Bjørkøy, G., and Johansen, T. (2007) p62/SQSTM1 binds directly to Atg8/LC3 to facilitate degradation of ubiquitinated protein aggregates by autophagy. *J. Biol. Chem.* **282,** 24131–24145 CrossRef Medline
53. Colecchia, D., Strambi, A., Sanzone, S., Iavarone, C., Rossi, M., Dall'Armi, C., Piccioni, F., Verrotti di Pianella, A., and Chiariello, M. (2012) MAPK15/ERK8 stimulates autophagy by interacting with LC3 and GABARAP proteins. *Autophagy* **8,** 1724–1740 CrossRef Medline
54. Lee, K. K., and Yonehara, S. (2002) Phosphorylation and dimerization regulate nucleocytoplasmic shuttling of mammalian STE20-like kinase (MST). *J. Biol. Chem.* **277,** 12351–12358 CrossRef Medline
55. Ni, L., Zheng, Y., Hara, M., Pan, D., and Luo, X. (2015) Structural basis for Mob1-dependent activation of the core Mst-Lats kinase cascade in Hippo signaling. *Genes Dev.* **29,** 1416–1431 CrossRef Medline
56. Parekh, D. B., Ziegler, W., and Parker, P. J. (2000) Multiple pathways control protein kinase C phosphorylation. *EMBO J.* **19,** 496–503 CrossRef Medline
57. Subramani, S., and Malhotra, V. (2013) Nonautophagic roles of autophagy-related proteins. *EMBO Rep.* **14,** 143–151 CrossRef Medline
58. Popovic, D., Akutsu, M., Novak, I., Harper, J. W., Behrends, C., and Dikic, I. (2012) Rab GTPase-activating proteins in autophagy: regulation of endocytic and autophagy pathways by direct binding to human ATG8 modifiers. *Mol. Cell. Biol.* **32,** 1733–1744 CrossRef Medline
59. Baisamy, L., Cavin, S., Jurisch, N., and Diviani, D. (2009) The ubiquitin-like protein LC3 regulates the Rho-GEF activity of AKAP-Lbc. *J. Biol. Chem.* **284,** 28232–28242 CrossRef Medline
60. Nguyen, T. N., Padman, B. S., Usher, J., Oorschot, V., Ramm, G., and Lazarou, M. (2016) Atg8 family LC3/GABARAP proteins are crucial for autophagosome–lysosome fusion but not autophagosome formation during PINK1/Parkin mitophagy and starvation. *J. Cell Biol.* **215,** 857–874 CrossRef Medline
61. Vaites, L. P., Paulo, J. A., Huttlin, E. L., and Harper, J. W. (2018) Systematic analysis of human cells lacking ATG8 proteins uncovers roles for GABARAPs and the CCZ1/MON1 regulator C18orf8/RMC1 in macroautophagic and selective autophagic flux. *Mol. Cell. Biol.* **38,** e00392–17 CrossRef Medline
62. Jain, A., Lamark, T., Sjøttem, E., Larsen, K. B., Awuh, J. A., Øvervatn, A., McMahon, A., Hayes, J. D., and Johansen, T. (2010) p62/SQSTM1 is a target gene for transcription factor NRF2 and creates a positive feedback

loop by inducing antioxidant response element-driven gene transcription. *J. Biol. Chem.* **285,** 22576–22591 CrossRef Medline

63. Pankiv, S., Alemu, E. A., Brech, A., Bruun, J. A., Lamark, T., Overvatn, A., Bjørkøy, G., and Johansen, T. (2010) FYCO1 is a Rab7 effector that binds to LC3 and PI3P to mediate microtubule plus end-directed vesicle transport. *J. Cell Biol.* **188,** 253–269 CrossRef Medline
64. Skytte Rasmussen, M., Mouilleron, S., Kumar Shrestha, B., Wirth, M., Lee, R., Bowitz Larsen, K., Abudu Princely, Y., O'Reilly, N., Sjøttem, E., Tooze, S. A., Lamark, T., and Johansen, T. (2017) ATG4B contains a C-terminal LIR motif important for binding and efficient cleavage of mammalian orthologs of yeast Atg8. *Autophagy* **13,** 834–853 CrossRef Medline
65. Kirkin, V., Lamark, T., Sou, Y. S., Bjørkøy, G., Nunn, J. L., Bruun, J. A., Shvets, E., McEwan, D. G., Clausen, T. H., Wild, P., Bilusic, I., Theurillat, J. P., Øvervatn, A., Ishii, T., Elazar, Z., *et al.* (2009) A role for NBR1 in autophagosomal degradation of ubiquitinated substrates. *Mol. Cell* **33,** 505–516 CrossRef Medline
66. Perez-Riverol, Y., Csordas, A., Bai, J., Bernal-Llinares, M., Hewapathirana, S., Kundu, D. J., Inuganti, A., Griss, J., Mayer, G., Eisenacher, M., Pérez, E., Uszkoreit, J., Pfeuffer, J., Sachsenberg, T., Yilmaz, S., *et al.* (2019) The PRIDE database and related tools and resources in 2019: improving support for quantification data. *Nucleic Acids Res.* **47,** D442–D450 CrossRef Medline